

¹ The effects of drought on land cover change and vegetation productivity in
² continental Chile

³ Francisco Zambrano^{a,b,*}, Anton Vrieling^c, Francisco Meza^{d,e,f}, Iongel Duran-Llacer^g, Francisco
⁴ Fernández^{h,i}, Alejandro Venegas-González^j, Nicolas Raab^d, Dylan Craven^{l,m}

^a Hémera Centro de Observación de la Tierra, Facultad de Ciencias, Escuela de Ingeniería en Medio Ambiente y Sustentabilidad, Universidad Mayor, Santiago, 7500994, Chile.,

^b Observatorio de Sequía para la Agricultura y la Biodiversidad de Chile (ODES), Universidad Mayor, Santiago, 7500994, Chile.,

^c Faculty of Geo-Information Science and Earth, University of Twente, Enschede, The Netherlands.,

^d Facultad de Agronomía y Sistemas Naturales, Pontificia Universidad Católica de Chile., Santiago, Chile.,

^e Instituto para el Desarrollo Sustentable. Pontificia Universidad Católica de Chile, Santiago, Chile.,

^f Centro Interdisciplinario de Cambio Global, Pontificia Universidad Católica de Chile, Santiago, Chile.,

^g Hémera Centro de Observación de la Tierra, Facultad de Ciencias, Universidad Mayor, Santiago, 7500994, Chile.,

^h Center of Economics for Sustainable Development (CEDES), Faculty of Economics and Government, Universidad San Sebastián, Santiago, Chile.,

ⁱ Center of Applied Ecology and Sustainability (CAPES), Santiago, Chile.,

^j Instituto de Ciencias Agroalimentarias, Animales y Ambientales (ICA3), Universidad de O'Higgins, San Fernando, Chile.,
k,

^l, GEMA Center for Genomics, Ecology & Environment, Universidad Mayor, Camino La Pirámide Huechuraba 5750, Santiago, Chile.,

^m Data Observatory Foundation, Santiago, Chile.,

⁵ **Abstract**

Chile has experienced a persistent decrease in water supply, which impacts the hydrological system and vegetation development. This persistent period of water scarcity has been defined as a mega-drought. There is yet insufficient understanding of ecological drought in Chile due to the limited studies on the relationship between drought and ecosystem changes. The aim of our study is to evaluate the interaction of drought, land cover change, and vegetation productivity over continental Chile. To assess drought, we used drought indices for atmospheric evaporative demand (AED), water supply, and soil moisture from short- (1, 3, 6 months) to long-term (12, 24, 36 months) time scales. We derived the drought indices using monthly ERA5-Land reanalysis data from 1981 to 2023. We used Moderate-Resolution Imaging Spectroradiometer (MODIS) datasets to derive information on annual land cover and monthly vegetation productivity. Our results showed that, except for the Austral part, Chile has a temporal decreasing trend in water supply, and across the whole country, there is an increase in AED. These trends become stronger over longer time scales. We found a negative trend in vegetation productivity in the north-central area, which is more prominent for shrubland and savanna as compared to croplands and forests. The anomaly in soil moisture over the past 12 months (SSI-12) is the most important variable explaining these changes, followed by anomalies in accumulated precipitation over one to two years (SPI-12 and SPI-24). The variable importance obtained by random forest models indicates that drought explains about 12–41% of the change in land cover surface across Chile for forest, grassland, shrubland, and savanna but has little relation to the changes in croplands. The increase in AED is the main variable associated with the change in land cover, followed by a reduction

in precipitation and soil moisture. Our findings provide insightful information that could assist in developing adaptation measures for Chilean ecosystems to cope with climate change and drought.

6 *Keywords:* drought, land cover change, vegetation productivity, ecosystem

7 **1. Introduction**

8 Drought can be classified as 1) meteorological, when precipitation in a specific period remains below the
9 mean precipitation experienced in the same period during multiple years (more than 30 years usually);
10 2) hydrological, when these anomalies last for long periods (months to years) and affect water systems;
11 and 3) agricultural, when the deficit negatively impacts plant health and leads to decreased productivity
12 of crops or pastures (Wilhite and Glantz, 1985). However, because drought is also influenced by human
13 activities, Van Loon et al. (2016) and AghaKouchak et al. (2021) expanded the drought definition for the
14 Anthropocene, indicating that the feedback of human decisions and activities should also be considered
15 (i.e., anthropogenic drought). Droughts can lead to increased tree mortality (Cheng et al., 2024) and induce
16 alterations in land cover and land use, ultimately affecting ecosystems (Crausbay et al., 2017). Even though
17 many ecological studies have at times mistakenly considered “dry” conditions as “drought” (Slette et al.,
18 2019), ecological drought can be defined as “*an episodic deficit in water availability that drives ecosystems*
19 *beyond thresholds of vulnerability, impacts ecosystem services, and triggers feedback in natural and/or human*
20 *systems*” (Crausbay et al., 2017). In light of current global warming, it is crucial to study the interaction
21 between drought and ecosystems in order to understand their feedback and impact on future water security
22 (Bakker, 2012).

23 Global warming, as a result of human-induced greenhouse gas emissions, has increased the frequency and
24 intensity of drought, according to the sixth assessment report (AR6) of the Intergovernmental Panel on
25 Climate Change (IPCC) (Calvin et al., 2023). The evidence supporting this claim has been strengthened
26 since AR5 (IPCC, 2013). Recent studies, however, have produced contrasting findings, with some suggesting
27 that drought has not exhibited a significant trend over the past forty years (Vicente-Serrano et al., 2022;
28 Kogan et al., 2020). Vicente-Serrano et al. (2022) analyzed the trend in meteorological drought on a global
29 scale, finding that only in a few regions an increase in the severity of drought was observed. Moreover,
30 they attributed this increase solely to an increase in atmospheric evaporative demand (AED) due to higher
31 temperatures, which in turn enhances vegetation water demand, with important implications for agricultural
32 and ecological droughts. Also, they state that “*the increase in hydrological droughts has been primarily*
33 *observed in regions with high water demand and land cover change, led by an increase in agricultural land*”.
34 Similarly, Kogan et al. (2020) analyzed the drought trend using remotely-sensed vegetation health indicators,
35 finding that for the globe and main grain-producing countries, drought has not expanded or intensified during
36 the past 38 years. Nonetheless, Masson-Delmotte (2021) suggests that there is a medium to high degree
37 of confidence that rising temperatures will increase the extent, frequency, and severity of agricultural and
38 ecological droughts. Also, AR6 (Calvin et al., 2023) predicts that many regions of the world will experience
39 more severe agricultural and ecological droughts even if global warming stabilizes at 1.5°–2°C. To better
40 evaluate the impact of drought trends on ecosystems, assessments of the relationship between meteorological
41 and soil moisture variables and their effects on vegetation are much needed.

42 From 1960 to 2019, land use change has impacted around one-third of the Earth’s surface, which is four
43 times more than previously thought (Winkler et al., 2021). Multiple studies aim to analyze and forecast
44 changes in land cover globally (Winkler et al., 2021; Song et al., 2018) and regionally (Chamling and Bera,
45 2020; Homer et al., 2020; Yang and Huang, 2021; Schulz et al., 2010; Echeverría et al., 2012). Some seek

*Corresponding author
Email address: francisco.zambrano@umayor.cl (Francisco Zambrano)

46 to analyze the impact of land cover change on climate conditions such as temperature and precipitation
47 (Luyssaert et al., 2014; Pitman et al., 2012). There is less research on drought and its relation to land cover
48 change and vegetation productivity (Chen et al., 2022; Akinyemi, 2021; Peng et al., 2017). Peng et al. (2017)
49 utilized net primary productivity to examine the spatial and temporal variations in vegetation productivity
50 at global level and assess to what extent drought influenced this variability by comparing the twelve-month
51 Standardized Precipitation Evapotranspiration Index (SPEI) and land cover change. According to their
52 findings, drought is responsible for 37% of the decline and accounts for 55% of the variability in vegetation
53 productivity. Chen et al. (2022) instead found poor correlations ($r < 0.2$) between the vegetation productivity
54 trends against meteorological drought (SPEI of twelve months in December) and soil moisture at the global
55 level. These studies mostly looked at how changes in land cover and vegetation productivity are related to a
56 single drought index (SPEI) obtained for 12 month periods. SPEI takes into account the combined effect of
57 precipitation and AED as a water balance, but it does not allow to know the contribution of each variable
58 on its own. To better understand these contributions on land cover change and vegetation productivity the
59 following questions may be asked: i) how do land cover and vegetation productivity respond to short- to
60 long-term meteorological and soil moisture droughts? And ii) how is this response different between humid
61 and arid climatic zones? Likewise, there is a lack of understanding of how the alteration in water supply
62 and demand is affecting land cover transformations.

63 To address the previous questions over extensive regions, we can utilize gridded data on water availability,
64 vegetation conditions, and the respective drought indices. For monitoring drought, the World Meteorological
65 Organization recommends the SPI (Standardized Precipitation Index) (WMO et al., 2012). The SPI is a
66 multi-scalar drought index that only uses precipitation to assess short- to long-term droughts. Vicente-
67 Serrano et al. (2010) proposed the Standardized Precipitation Evapotranspiration Index (SPEI), which
68 incorporates the temperature effect by subtracting AED from precipitation. SPEI allows for analyzing the
69 combined effect of precipitation and AED. Since its formulation, it has been used worldwide for the study and
70 monitoring of drought (Gebrechorkos et al., 2023; Liu et al., 2024). Recently, there has been more interest
71 in using AED to track droughts separately to better disentangle precipitation from temperature-dependent
72 effects (Vicente-Serrano et al., 2020). One of the reasons is that AED is more linked to flash droughts in
73 water-limited regions (Noguera et al., 2022). Hobbins et al. (2016) and McEvoy et al. (2016) developed the
74 Evaporative Demand Drought Index (EDDI) to monitor droughts solely using the AED, and it has proven
75 effective in monitoring flash droughts (Li et al., 2024; Ford et al., 2023). For soil moisture, several drought
76 indices exist, such as the Soil Moisture Deficit Index (SMDI) (Narasimhan and Srinivasan, 2005) and the
77 Soil Moisture Agricultural Drought Index (SMADI) (Souza et al., 2021). Hao and AghaKouchak (2013) and
78 AghaKouchak (2014) proposed the Standardized Soil Moisture Index (SSI), which has a similar formulation
79 as the SPI, SPEI, and EDDI. Thus, many drought indices exist that allow for a comprehensive assessment
80 of drought on short- to long-term scales and that allow for the use of single variables from Earth's water
81 balance (e.g., precipitation, AED, soil moisture). Climatic variability impacts vegetation development, with
82 unfavorable conditions such as low precipitation and high temperatures usually promoting a decrease in plant
83 productivity. To monitor the response of vegetation for large areas, the common practice is to use satellite
84 data. For example, the Normalized Difference Vegetation Index (NDVI) derived from frequent satellite
85 observations of red and near infrared spectral reflectance, has been widely used as a proxy for biomass
86 production [Camps-Valls et al. (2021); Paruelo et al. (2016); Helman et al. (2014)]. For Chile's cultivated
87 land, Zambrano et al. (2018) used the zcNDVI for assessing seasonal biomass production in response to
88 drought. Comparing the various meteo-related and vegetation-based drought indices, we can further our
89 understanding of the impact of drought on ecosystems.

90 Chile's diverse climatic and ecosystem types (Beck et al., 2023; Luebert and Pliscoff, 2022) make it an
91 ideal natural laboratory for studying climate and ecosystems. Additionally, the country has experienced
92 severe drought conditions that have had significant effects on vegetation and water storage. North-central
93 Chile has faced a persistent precipitation deficit since 2010, defined as a mega-drought (Garreaud et al.,
94 2017), which has impacted the Chilean ecosystem and consequently makes it highly vulnerable to climate
95 change (Barria et al., 2021; Alvarez-Garretón et al., 2021). This mega-drought was defined by the annual
96 time series of the Standardized Precipitation Index (SPI) at a time scale of twelve months at the end of

97 each year (December) when having values below one standard deviation. Some studies have addressed how
98 this drought affects single ecosystems in terms of forest growth ([Miranda et al., 2020](#); [Venegas-González et al., 2018](#)), forest fire occurrence ([Urrutia-Jalabert et al., 2018](#)), and crop productivity ([Zambrano, 2023b; Zambrano et al., 2018](#), [Zambrano et al. \(2016\)](#)). The term “mega-drought” is used in Chile to describe
100 a prolonged water shortage that lasts for several years, resulting in a permanent deficit that impacts the
101 hydrological system ([Boisier et al., 2018](#)). Therefore, it is crucial to evaluate temporal scales that consider
102 the cumulative impact over a period of several years. In Chile, the relationship between drought and the
103 environment remains poorly understood. Hence, we aim to contribute to understanding how climatic and
104 soil moisture droughts influence ecosystem dynamics in order to provide useful information that helps for
105 a better understanding of ecological droughts and, at the same time, helps to make well-informed decisions
106 on adaptation strategies.

108 Here, we analyze the multi-dimensional impacts of drought across ecosystems in continental Chile. More
109 specifically, we aim to assess: i) short- to long-term temporal trends in multi-scalar drought indices; ii)
110 temporal changes in land-use cover and the direction and magnitude of their relationships with trends in
111 drought indices; and iii) the trend in vegetation productivity and its relationship with drought indices across
112 Chilean ecosystems.

113 2. Study area

114 Continental Chile has diverse climate conditions with strong gradients from north to south and east to
115 west ([Aceituno et al., 2021](#)) Figure 1a, which determines its great ecosystem diversity ([Luebert and Pliscoff, 2022](#))
116 (Figure 1c). The Andes Mountains are a main factor in climate variation ([Garreaud, 2009](#)). For an aggregated
117 overview of the results of the study, we used the five Chilean macrozones: “Norte Grande” (17°34’–
118 25°42’S), “Norte Chico” (25°42’–32°8’S), “Centro” (32°08’–36°12’S), “Sur” (36°12’–43°48’S), and “Austral”
119 (43°48’–56°00’S). “Norte Grande” and “Norte Chico” predominate in an arid desert climate with hot (Bwh)
120 and cold (Bwk) temperatures. At the south of “Norte Chico”, the climate changes to an arid steppe with
121 cold temperatures (Bsk). In these two northern regions, the land is mostly bare, with a small surface of
122 vegetation types such as shrubland and grassland. In the macrozones “Centro” and the northern half of
123 “Sur”, the main climate is Mediterranean, with warm to hot summers (Csa and Csb). Land cover in “Centro”
124 comprises a significant amount of shrubland and savanna (50%), grassland (16%), forest (8%), and
125 croplands (5%). An oceanic climate (Cfb) predominates in the south of “Sur” and the north of “Austral”.
126 Those zones have a large area of forest and grassland. The southern part of the country has a tundra
127 climate, while “Austral” is a cold semi-arid area with an extended surface of grassland, forest, and, to a
128 lesser extent, savanna.

129 3. Materials and Methods

130 3.1. Data

131 3.1.1. Gridded meteorological and vegetation data

132 To analyze land cover change, we used the classification scheme by the IGBP (International Geosphere-
133 Biosphere Programme) from the product MCD12Q1 Collection 6.1 from MODIS. The MCD12Q1 product
134 is produced for each year from 2001 to 2022 and defines 17 classes (see Table S1). To maintain our focus
135 on a large scale and follow the FAO classification ([FAO, 2022](#)), we considered native and planted forests as
136 “forests”, which represent ecosystems dominated by larger trees. To derive a proxy for vegetation produc-
137 tivity, we used the Normalized Difference Vegetation Index (NDVI) from the product MOD13A3 Collection
138 6.1 from MODIS ([Didan, 2015](#)). MOD13A3 provides vegetation indices with 1km spatial resolution and
139 monthly frequency. The NASA EOSDIS Land Processes Distributed Active Archive Center (LP DAAC),

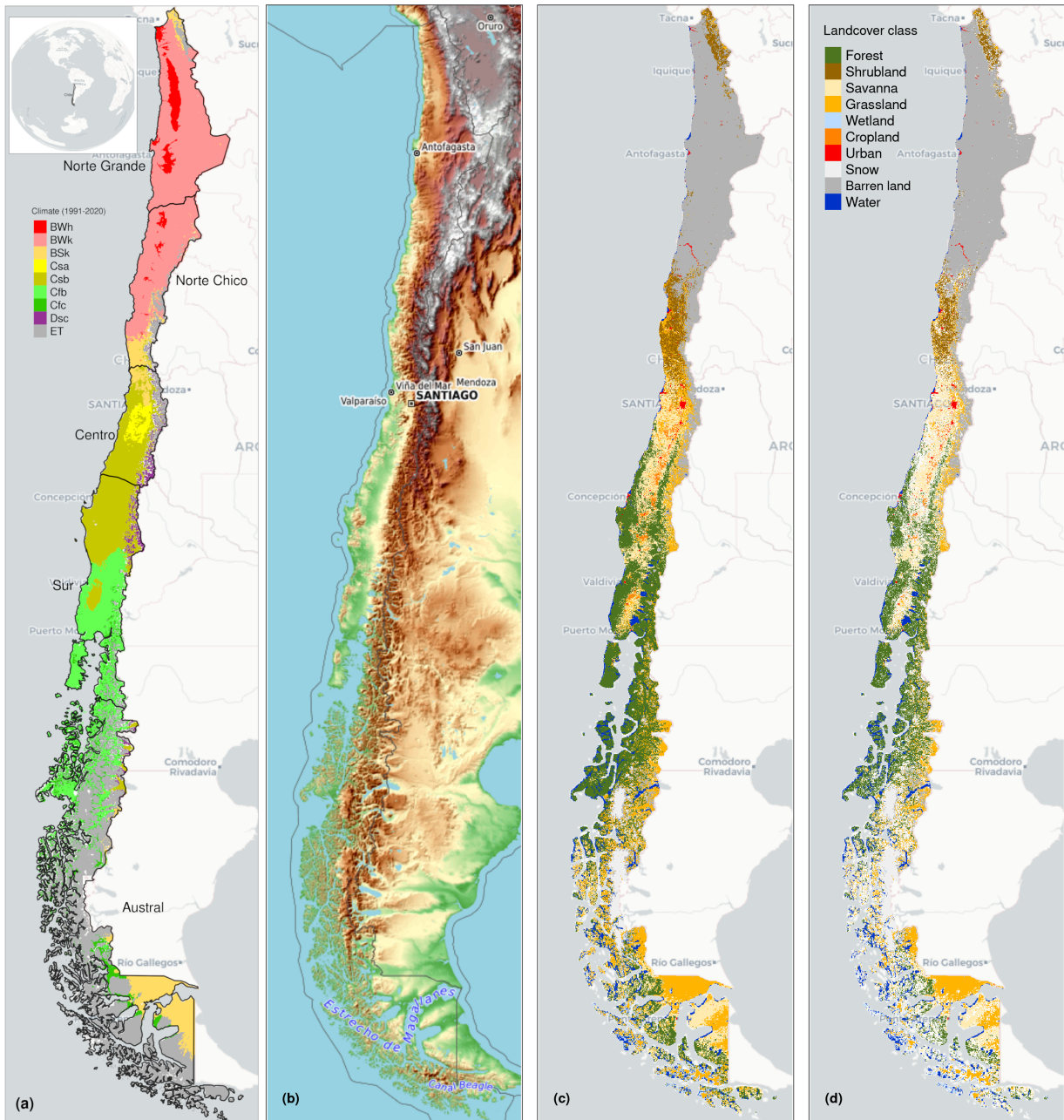


Figure 1: (a) Chile with the Koppen-Geiger climate classes and the five macrozones “Norte Grande”, “Norte Chico”, “Centro”, “Sur”, and “Austral”. (b) Topography reference map. (c) land cover classes for 2022. (d) Persistent land cover classes (> 80%) for 2001-2022

140 USGS Earth Resources Observation and Science (EROS) Center, Sioux Falls, South Dakota, provided the
 141 MOD13A3 and MCD12Q1 from the online Data Pool, accessible at <https://lpdaa.usgs.gov/tools/data-pool/>.
 142 For soil moisture, water supply, and water demand variables, we used ERA5-Land (ERA5L) (ECMWF
 143 Reanalysis version 5 over land) ([Muñoz-Sabater et al., 2021](#)), a reanalysis dataset that provides the evolution
 144 of atmospheric and land variables since 1950. It has a spatial resolution of 0.1° (9 km), hourly frequency,

Table 1: Description of the satellite and reanalysis data used

Product	Sub-product	Variable	Spatial Resolution	Period	Units	Short Name
ERA5L		Precipitation	0.1°	1981-2023	mm	P
		Maximum temperature			°C	T_{max}
		Minimum temperature			°C	T_{min}
ERA5L*		Volumetric Soil Water Content at 1m	0.1°	1981-2023	m3/m3	SM
		Atmospheric Evaporative Demand			mm	AED
MODIS	MOD13A3.061	Normalized Difference Vegetation Index	1 km	2000-2023	mm	NDVI
	MCD12Q1.061	land cover IGBP scheme		2001-2022	land cover	

*Calculated from maximum and minimum temperatures derived from ERA5L with Eq. 1.

145 and global coverage. We selected the variables for total precipitation, maximum and minimum temperature
146 at 2 meters, and volumetric soil water layers between 0 and 100 cm of depth (layer 1 to layer 3). Table 1
147 shows a summary of the data and its main characteristics.

148 *3.2. Short- to long-term drought trends*

149 *3.2.1. Atmospheric Evaporative Demand (AED)*

150 To compute the drought indices that use water demand, it is necessary to first calculate the AED. To do
151 this, we employed the Hargreaves method (Hargreaves, 1994; Hargreaves and Samani, 1985) by applying the
152 following equation:

$$AED = 0.0023 \cdot Ra \cdot (T + 17.8) \cdot (T_{max} - T_{min})^{0.5} \quad (1)$$

153 where Ra ($MJ\ m^2\ day^{-1}$) is extraterrestrial radiation; T , T_{max} , and T_{min} are mean, maximum, and
154 minimum temperature ($^{\circ}C$) at 2m. For calculating Ra we used the coordinate of the latitud of the centroid
155 of each pixel as follow:

$$Ra = \frac{14,400}{\pi} \cdot G_{sc} \cdot d_r [\omega_s \cdot \sin(\phi) \cdot \sin(\delta) + \cos(\phi) \cdot \cos(\delta) \cdot \sin(\omega_s)] \quad (2)$$

156 where:

157 Ra : extraterrestrial radiation [$MJ\ m^{-2}\ day^{-1}$],

158 G_{sc} : solar constant = 0.0820 [$MJ\ m^{-2}\ min^{-1}$],

159 d_r : inverse relative distance Earth-Sun,

160 ω_s : sunset hour angle [rad],

161 ϕ : latitude [rad],

162 δ : solar declination [rad].

163 We chose the method of Hargreaves to estimate AED because of its simplicity, which only requires tem-
164 peratures and extrarrestrial radiation. Also, it has been recommended over other methods (e.g., Penman-
165 Monteith) when the access to climatic variables is limited (Vicente-Serrano et al., 2014).

166 *3.2.2. Non-parametric calculation of drought indices*

167 To derive the drought indices of water supply and demand, soil moisture, and vegetation (i.e., the proxy
168 of productivity), we used the ERA5L dataset and the MODIS product, with a monthly frequency for 1981–
169 2023 and 2000–2023, respectively. The drought indices correspond to a historical anomaly of a variable (e.g.,
170 meteorological, vegetation, or soil moisture). To account for the anomaly, the common practice is to derive
171 it following a statistical parametric method in which it is assumed that the statistical distribution of the
172 data is known (Heim, 2002). The use of an erroneous statistical distribution that does not fit the data is

173 usually the highest source of uncertainty (Laimighofer and Laaha, 2022). In the case of Chile, due to its
 174 high degree of climatic variability, it is difficult to choose a proper distribution without previous research
 175 that could be applicable throughout Chile. Here, we follow a non-parametric method for the calculation
 176 of the drought indices, in a similar manner as the framework proposed by Farahmand and AghaKouchak
 177 (2015).

178 For the purpose of monitoring water supply drought, we used the well-known Standardized Precipitation
 179 Index (SPI), which relies on precipitation data. To evaluate water demand, we chose the Evaporative
 180 Demand Drought Index (EDDI), developed by Hobbins et al. (2016) and McEvoy et al. (2016), which is based
 181 on the AED. The United States currently monitors drought using the EDDI (<https://psl.noaa.gov/eddi/>) as
 182 an experimental index. To consider the combined effect of water supply and demand, we selected the SPEI
 183 (Vicente-Serrano et al., 2010). For SPEI, an auxiliary variable $D = P - AED$ is calculated. Soil moisture is
 184 the main driver of vegetation productivity, particularly in semi-arid regions (Li et al., 2022). Hence, for soil
 185 water drought, we used the SSI (Standardized Soil Moisture Index) (Hao and AghaKouchak, 2013). For the
 186 SSI, we used the average soil moisture from ERA5L at 1m depth. Finally, for the proxy of productivity, we
 187 used the zcNDVI (Zambrano et al., 2018), which was derived from the monthly time series of NDVI derived
 188 from MOD13A1. All the indices are multi-scalar and can be used for the analysis of short- to long-term
 189 droughts.

190 To derive the drought indices, we first calculate the sum of the variables with regard to the time scale(s).
 191 In this case, for generalization purposes, we will use V , referring to variables P , AED , D , $NDVI$, and SM
 192 (Table 1). We accumulated each over the time series of values (months), and for the time scales s :

$$A_i^s = \sum_{i=n-s-i+2}^{n-i+1} V_i \quad \forall i \geq n - s + 1 \quad (3)$$

193 The A_i^s corresponds to a moving window (convolution) that sums the variable for time scales s . This
 194 summation is done over s months, starting from the most recent month (n) back in time until month
 195 $n - s + 1$. For example, using as a variable the precipitation, a period of twelve months (n), and a time scale
 196 of three months (s), it will be:

$$\begin{aligned} A_1^3 &= P_{oct} + P_{nov} + P_{dic} \\ &\vdots = \vdots + \vdots + \vdots \\ A_{10}^3 &= P_{jan} + P_{feb} + P_{mar} \end{aligned}$$

197 Then, we used the empirical Tukey plotting position (Wilks, 2011) over A_i^s to derive the $P(A_i^s)$ probabilities
 198 across a period of interest:

$$P(A_i^s) = \frac{i - 0.33}{n + 0.33} \quad (4)$$

199 An inverse normal approximation (Abramowitz and Stegun, 1968) obtains the empirically derived proba-
 200 bilities once the variable cumulates over time for the scale s . Thus, the drought indices SPI, SPEI, EDDI,
 201 SSI, and zcNDVI and obtained following the equation:

$$DI(A_i^s) = W - \frac{C_0 + C_1 \cdot W + c_2 \cdot W^2}{1 + d_1 \cdot W + d_2 \cdot W^2 + d_3 \cdot W^3} \quad (5)$$

202 DI is referring to the drought index calculated for the variable V (i.e., SPI, SPEI, EDDI, SSI, and zcNDVI).
 203 The values for the constats are: $C_0 = 2.515517$, $C_1 = 0.802853$, $C_2 = 0.010328$, $d_1 = 1.432788$, $d_2 =$

204 0.189269, and $d3 = 0.001308$. For $P(A_i^s) \leq 0.5$, $W = \sqrt{-2 \cdot \ln(P(A_i^s))}$, and for $P(A_i^s) > 0.5$, replace $P(A_i^s)$
205 with $1 - P(A_i^s)$ and reverse the sign of $DI(A_i^s)$.

206 The drought indices were calculated for time scales of 1, 3, 6, 12, 24, and 36 months at a monthly frequency
207 for 1981–2023 in order to be used for short- to long-term evaluation of drought.

208 For the proxy of vegetation productivity, we chose the time scale that best correlates with annual net
209 primary productivity (NPP) across continental Chile. For this purpose, we calculated the zcNDVI for time
210 scales of 1, 3, 6, and 12 months in December and compared it with the annual NPP. We used the NPP
211 from the MOD17A3HGF ([Running and Zhao, 2019](#)) dataset (MODIS). We chose to use six months because
212 the R^2 between zcNDVI and NPP reaches its highest value at six months. We obtained an R^2 of 0.31 for
213 forest and 0.72 for shrubland (refer to the supplementary material in Section S5). Then, we chose the proxy
214 of vegetation productivity for six months, which we will name zcNDVI hereafter. It was calculated at a
215 monthly frequency for 2000–2023.

216 3.2.3. Trend of drought indices

217 To estimate if there are significant positive or negative trends for the drought indices, we used the non-
218 parametric Mann-Kendall test ([Kendall, 1975](#)). To determine the magnitude of the trend, we used Sen's
219 slope ([Sen, 1968](#)). Sen's slope has the advantage over normal regression that it is less affected by outliers,
220 and as a non-parametric method it is not influenced by the distribution of the data. We applied the Mann-
221 Kendall test to see if the trend was significant and Sen's slope to estimate the magnitude of the trend.
222 We did this for the indices SPI, EDDI, SPEI, and SSI using the six time scales with data from 1981 to
223 2023 (monthly frequency), resulting in 24 trends (per index and time scale). Then, we extracted the trend
224 aggregated by each of the five macrozones: “Norte Grande” to “Austral”, and per land cover type: grassland,
225 forest, cropland, shrubland, savanna, and barren land (Figure 1d).

226 3.3. Interaction of land cover and drought

227 3.3.1. Land cover change

228 To analyze the land cover change, we use the IGBP scheme from the MCD12Q1 Collection 6.1 from
229 MODIS. This product has been previously used for studies of drought and land cover in Chile ([Fuentes](#)
230 [et al., 2021](#); [Zambrano et al., 2018](#)). We regrouped the 17 classes into ten macroclasses, as follows: classes
231 1-4 to forest, 5-7 to shrublands, 8-9 to savannas, 10 as grasslands, 11 as wetlands, 12 and 14 to croplands, 13
232 as urban, 15 as snow and ice, 16 as barren, and 17 to water bodies (Table S1). Thus, we have a land cover
233 raster time series with the ten macroclasses for 2001 and 2023. We validate the land cover macroclasses
234 regarding a highly detailed (30 m of spatial resolution) land cover map made for Chile by [Zhao et al. \(2016\)](#)
235 for 2013-2014. Our results showed a global accuracy of ~0.82 and a F1 score of ~0.66. Section S2 in the
236 Supplementary Material shows the procedure for validation.

237 We calculated the surface occupied per land cover class into the five macrozones (“Norte Grande” to
238 “Austral”) per year for 2001–2022. After that, we calculated the trend's change in surface per land cover
239 type and macroclass. We used Mann-Kendall for the significance of the trend ([Kendall, 1975](#)) and Sen's
240 slope to calculate the magnitude ([Sen, 1968](#)).

241 To assess how water demand and supply, and soil moisture affect the variation in vegetation productivity
242 across various land cover types, we avoid analyzing areas that experienced major land cover changes in
243 the 2021–2022 period. To assess how zcNDVI varied irrespective of land cover change, we developed a
244 persistence mask for land cover, which only retains pixels for which the macroclass remained the same for
245 at least 80% of the 22 years (Figure 1d).

246 3.3.2. Relationship between land cover and drought trends

247 To identify which drought indices and time scales have a major impact on changes in land cover type, we
248 examined the relationship between the trend in land cover classes and the trend in drought indices. To have
249 more representative results, we conducted the analysis over sub-basins within continental Chile. We used
250 469 basins, which have a surface area between 0.0746 and 24,000 km² and a median area of 1,249 km². For
251 each basin, we calculated the trend per land cover type, considering the proportion of the type relative to
252 the total surface of the basin. Then, we extracted per basin the average trend (Sen's slope) of the drought
253 indices SPI, SPEI, EDDI, SSI, and all their time scales 1, 3, 6, 12, 24, and 36. Also, we extracted the average
254 trend in the proxy of vegetation productivity (zcNDVI).

255 We model the trends in land cover per macroclass with the aim of assessing how land cover trends relate
256 to drought indices. We used the random forest method ([Ho, 1995](#)), which employs multiple decision trees,
257 allowing for classification and regression. Some advantages include the ability to find non-linear relationships,
258 reduce overfitting, and derive variable importance. We included the four drought indices per six time scales
259 and the zcNDVI, totaling 25 predictors. As a result, we created thirty random forest models, one for each
260 land cover macroclass trend and per macrozone. Each model was trained using 1000 forests in a resampling
261 scheme to obtain more reliable results regarding variable importance. We resampled by creating ten folds,
262 running a random forest per fold, and calculating the R^2 , root mean square error (RMSE), and variable
263 importance. The variable importance helps for a better understanding of the relationships by finding which
264 variable has a higher contribution to the model. Thus, we calculated the variable's importance by permuting
265 out-of-bag (OOB) data per tree and computing the mean standard error in the OOB. After permuting each
266 predictor variable, we repeated the process for the remaining variable. We repeated this process ten times
267 (per fold) to obtain the performance metrics (R^2 , RMSE, and variable importance).

268 Finally, we visually explored the connection between the SPI, EDDI, and SSI drought indices for short-
269 and long-term changes in land cover. To do this, we compared the relative changes in land cover surface
270 (in terms of the total surface area per land cover type and macrozone) with the drought indices of six
271 (short-term) and thirty-six months (long-term).

272 3.4. Drought impacts on vegetation productivity

273 For each land cover macroclass, we analyzed the trend of vegetation productivity over the unchanged land
274 cover macroclasses. To achieve this, we used the persistent mask of land cover macroclasses, thus reducing
275 the possibility of evaluating productivity trends that are due to year-to-year variation in land cover. We
276 used the zcNDVI as a proxy of vegetation productivity. To assess productivity in Chile's cultivated land,
277 [Zambrano et al. \(2018\)](#) used the zcNDVI for assessing seasonal biomass production in relation to climate.

278 We examined the drought indices of water demand, water supply, and soil moisture and their correlation
279 with vegetation productivity. The objective is to determine to what extent soil moisture and water demand
280 and supply affect vegetation productivity, thus addressing three main questions: 1) Which of the drought
281 variables—supply, demand, or soil moisture—helps most in explaining the changes in vegetation productivity?
282 2) How do the short- to long-term time scales of the drought variable affect vegetation productivity
283 in Chile, and how strong is the relationship? And finally, 3) how does the correlation vary per-land cover
284 type? Answering these questions should advance our understanding of how climate is affecting vegetation,
285 considering the impact on the five land cover types: forest, cropland, grassland, savanna, and shrubland.

286 We conducted an analysis on the linear correlation between the indices SPI, SPEI, EDDI, and SSI over
287 time periods of 1, 3, 6, 12, 24, and 36 months with zcNDVI. We used a method similar to that used by
288 [Meroni et al. \(2017\)](#) which compared the SPI time-scales with the cumulative fAPAR (fraction of Absorbed
289 Photosynthetically Active Radiation). We performed a pixel-to-pixel linear correlation analysis for each
290 index within the persistent mask of land cover macroclasses. We first compute the Pearson coefficient of
291 correlation for each of the six time scales. A time scale is identified as the one that attains the highest
292 correlation ($p < 0.05$). We then extracted the Pearson correlation coefficient corresponding to the time

²⁹³ scales where the value peaked. As a result, for each index, we generated two raster maps: 1) containing
²⁹⁴ the raster with values of the time scales and drought index that reached the maximum correlation, and 2)
²⁹⁵ having the magnitude of the correlation obtained by the drought index at the time scales.

²⁹⁶ *3.5. Software*

²⁹⁷ For the downloading, processing, and analysis of the spatio-temporal data, we used the open source software
²⁹⁸ for statistical computing and graphics, R ([R Core Team, 2023](#)). For downloading ERA5L, we used the
²⁹⁹ {ecmwfr} package ([Hufkens et al., 2019](#)). For processing raster data, we used {terra} ([Hijmans, 2023](#)) and
³⁰⁰ {stars} ([Pebesma and Bivand, 2023](#)). For managing vectorial data, we used {sf} ([Pebesma, 2018](#)). For the
³⁰¹ calculation of AED, we used {SPEI} ([Beguería and Vicente-Serrano, 2023](#)). For mapping, we used {tmap}
³⁰² ([Tennekes, 2018](#)). For data analysis and visualization, the suite {tidyverse} ([Wickham et al., 2019](#)) was
³⁰³ used. For the random forest modeling, we used the {tidymodels} ([Kuhn and Wickham, 2020](#)) and {ranger}
³⁰⁴ ([Wright and Ziegler, 2017](#)) packages.

³⁰⁵ **4. Results**

³⁰⁶ *4.1. Short- to long-term drought trends*

³⁰⁷ Figure 2 shows the spatial variation of the trend for the drought indices from short- to long-term scales.
³⁰⁸ SPI and SPEI have a decreasing trend from “Norte Chico” to “Sur”, but an increasing trend in “Austral”.
³⁰⁹ The degree of the trend is larger at higher time scales. In “Norte Grande”, the SSI increased in the southwest
³¹⁰ and decreased in the northeast, for all time scales. Similar to SPI and SPEI, SSI decreases at higher time
³¹¹ scales. EDDI showed a positive trend for the whole of continental Chile, with a higher slope toward the
³¹² north and a descending gradient toward the south. The slope of trend increases at higher time scales.

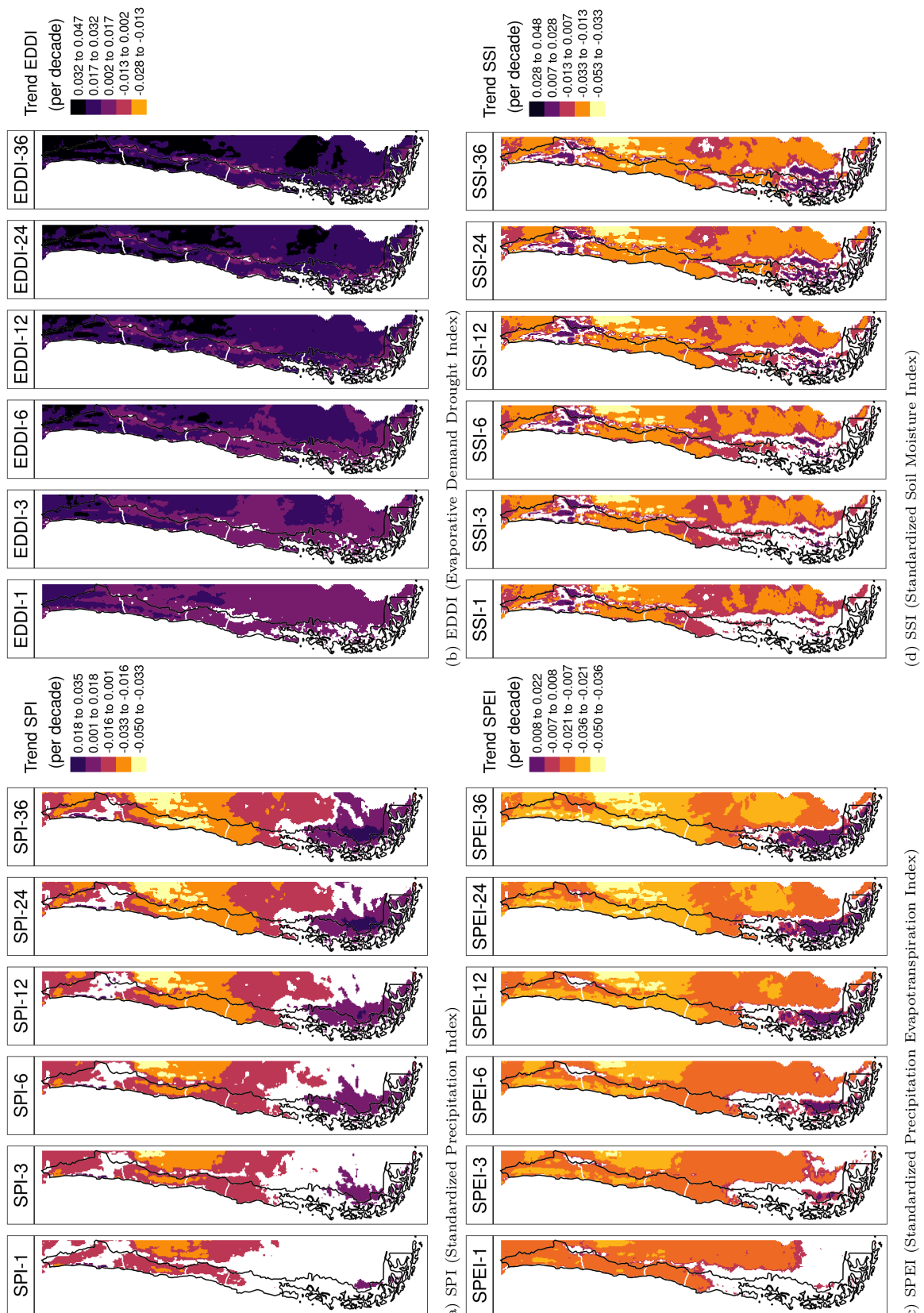


Figure 2: Linear trend of the drought index (*) at time scales of 1, 3, 6, 12, 24, and 36 months for 1981-2023

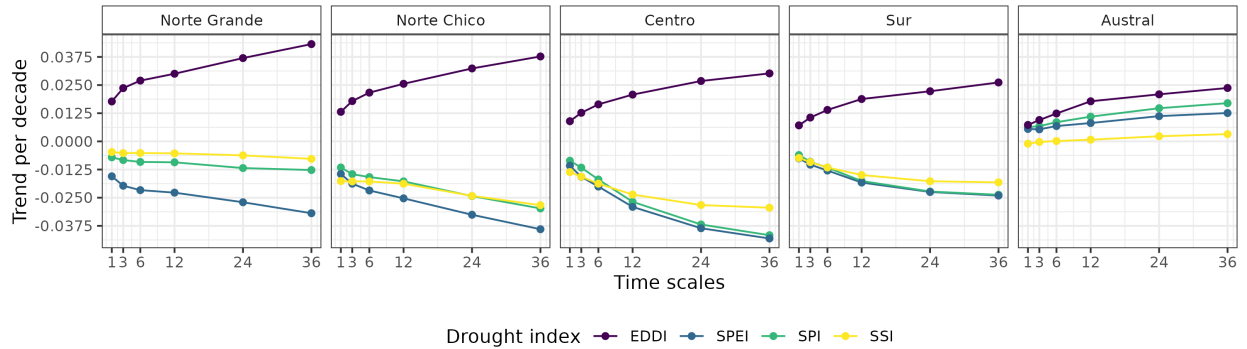


Figure 3: Trend per decade for the drought indices SPI, EDDI, SPEI, and SSI aggregated by macrozone.

313 The Figure 3 displays the aggregated trend per macrozone, drought index, and timescale. The macrozones
 314 that reached the lowest trend for SPI, SPEI, and SSI are “Norte Chico” and “Centro”, where the indices also
 315 decrease at longer time scales. This may potentially be explained by the prolonged reduction in precipitation
 316 that has affected the hydrological system in Chile. At 36 months, it reaches trends between -0.03 and -0.04
 317 (z-score) per decade for SPI, SPEI, and SSI. For “Sur”, the behavior is similar, decreasing at longer scales
 318 and having between -0.016 and -0.025 per decade for SPI, SPEI, and SSI. “Norte Grande” has the highest
 319 trend at 36 months for EDDI (0.042 per decade), and “Centro” has the lowest for SPI and SPEI. In “Norte
 320 Grande” and “Norte Chico”, which are in a semi-arid climate, it is evident that the EDDI has an effect on
 321 the difference between the SPI and SPEI index, which is not seen in the other macrozones. Contrary to
 322 the other macrozones, “Austral” showed an increase in all indices, being the highest for EDDI at 36 months
 323 (0.025) and the lowest for SSI, which shows only a minor increase in the trend.

324 4.2. Interaction of land cover and drought

325 4.2.1. Land cover change

Table 2: Surface per land cover class that persists during 2001–2022.

Surface [km ²]						
Macrozone	Forest	Cropland	Grassland	Savanna	Shrubland	Barren land
Norte Grande		886		7,910	171,720	
Norte Chico	90	4,283	589	16,321	84,274	
Centro	3,739	1,904	7,584	19,705	844	12,484
Sur	72,995	1,151	7,198	15,906		2,175
Austral	60,351		54,297	19,007	249	7,218
Total	137,085	3,145	74,247	55,206	25,324	277,870

326 For vegetation, we obtained and used hereafter five macroclasses of land cover from IGBP MODIS: forest,
 327 shrubland, savanna, grassland, and croplands. Figure 1c shows the spatial distribution of the macroclasses
 328 through Chile for the year 2022. Figure 1d shows the macroclasses of land cover persistence (80%) during
 329 2021–2022, respectively (Table 2). Within continental Chile, barren land is the land cover class with the
 330 highest surface area ($277,870 \text{ km}^2$). The largest type of vegetation, with $137,085 \text{ km}^2$, is forest. Grassland
 331 has $74,247 \text{ km}^2$, savanna $55,206 \text{ km}^2$, shrubland $25,324 \text{ km}^2$, and cropland $3,145 \text{ km}^2$ (Table 2). The
 332 macrozones with major changes for 2001–2022 were “Centro”, “Sur”, and “Austral”, with 36%, 31%, and
 333 34% of their surface changing the type of land cover, respectively (Figure 1 and Table 3). Figure 4 shows
 334 the variation for 2001–2022 in the proportion of surface per land cover class and macrozone, derived from
 335 the persistence mask over continental Chile.

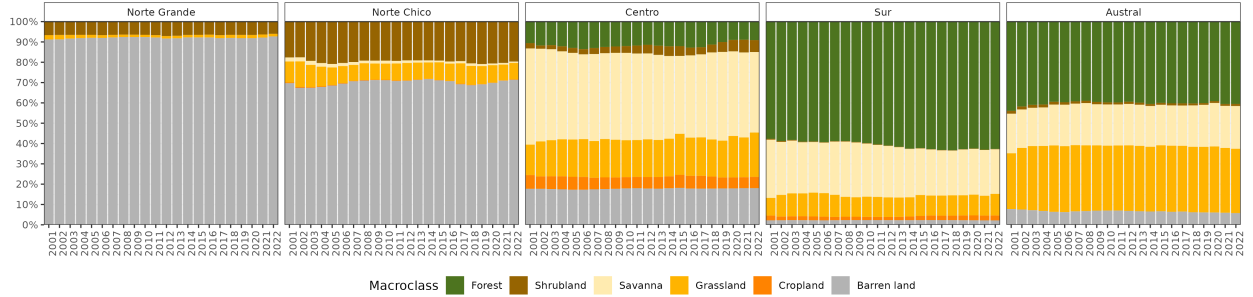


Figure 4: Proportion of land cover class from the persistent land cover for 2001–2022 (>80%) per macrozone and land cover macroclass.

Table 3: The value of Sen's slope trend next to the time-series plot of surface per land cover class (IGBP MCD12Q1.016) for 2001–2022 through Central Chile. Values of zero indicate that there was not a significant trend. The red dots on the plots indicate the maximum and minimum values of the surface. The white cells indicate that the landcover class is not significant in terms of surface area.

Trend of change [$\text{km}^2 \text{ year}^{-1}$]						
Macrozone	Forest	Cropland	Grassland	Savanna	Shrubland	Barren land
Norte Grande				0		0
Norte Chico		-12	0	-70	0	111
Centro	0	-22	83	-136	146	23
Sur	397	38	0	-319		0
Austral	0		0	172	-37	-93

336 From the trend analysis in Table 3, we can indicate that the “Norte Chico” shows an increase in barren
 337 land of $111 \text{ km}^2 \text{ yr}^{-1}$ and a reduction in the class savanna of $70 \text{ km}^2 \text{ yr}^{-1}$. In the “Centro” and “Sur”, there
 338 are changes with an important reduction in savanna with 136 and $319 \text{ km}^2 \text{ yr}^{-1}$, respectively, and an increase
 339 in shrubland and grassland, showing a change for more dense vegetation types. The area under cultivation
 340 (croplands) appears to be shifting from the “Centro” to the “Sur”. Also, there is a high increase in forest
 341 ($397 \text{ km}^2 \text{ yr}^{-1}$) in the “Sur”, seemingly replacing the savanna lost (Table 3).

342 4.2.2. Relationship between drought indices and land cover change

Table 4: The five most important trends of drought indices in estimating the landcover trend per land cover type and the R^2 reached by each random forest model. The white cells indicate that the landcover class is not significant in terms of surface area.

Macrozone	Forest	Cropland	Grassland	Savanna	Shrubland	Barren Land
Norte Grande		SPEI-36		SPI-36	EDDI-6	
Norte Chico	SPI-24	EDDI-6	EDDI-36	SPI-36	EDDI-6	
Centro	EDDI-3	SPI-24	SPEI-36	SPI-36	SPI-36	EDDI-6
Sur	EDDI-3	SPI-24	EDDI-6	SPI-36		EDDI-6
Austral	EDDI-36		SPEI-36	EDDI-12	SPI-36	EDDI-6

r-square: 0.12 0.22 0.32 0.42 0.52

343 Table 4 shows the drought indices that are the most important variables in the random forest models,
 344 together with the R^2 reached. The random forest models reached an R^2 between 0.12 and 0.41 for the land

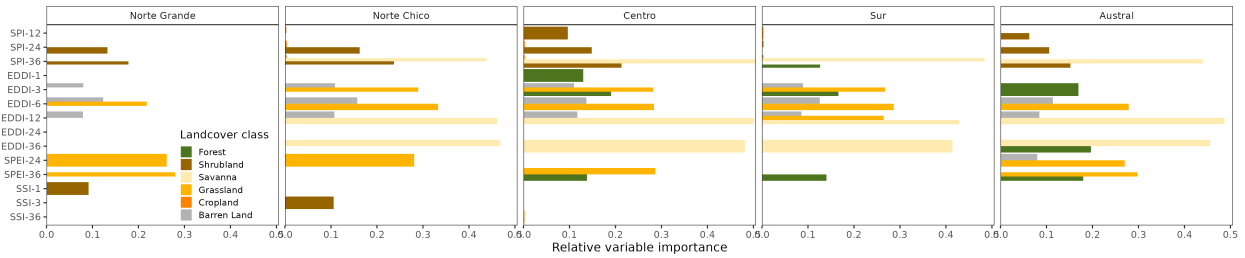


Figure 5: Relative importance of drought indices for explaining the trend in landcover change across the five macrozones in Chile. SPI, Standardized Precipitation Index; EDDI, Evaporative Demand Drought Index; SPEI, Standardized Precipitation Evapotranspiration Index; SSI, Standardized Soil Moisture Index. The numbers beside the drought index correspond to the time scales.

345 cover types and macrozones. The model shows the highest R^2 for shrublands (0.28 to 0.42) and the lowest
 346 R^2 for croplands (0.16 to 0.20) across all macrozones.

347 Figure 5 shows the three most important variables for the models across the five macrozones and per
 348 landcover type. For shrublands, the SPI of long-term and short-term SSI were the most relevant drought
 349 indices within the five macrozones. We showed that the trend in short-term EDDI (1–6 months) and long-
 350 term SPI (24- and 36-months) affected grasslands and forest changes. We showed that trends in SPI-36
 351 and long-term trends in EDDI (12 to 36 months) were associated with changes in savannas. The changes
 352 in barren land are shown to be limited to the changes in the short-term AED (1 to 6 months). Changes in
 353 croplands have not been linked to drought across all macrozones. The supplementary material in Section
 354 S3 provides further details about the variable's importance.

355 Figure 6 shows the connection between the SPI, EDDI, and SSI drought indices for time scales of 6 and 36
 356 months against changes in land cover. Forest in the “Sur”, shrubland and grassland in “Centro”, barren land
 357 in “Norte Chico”, and savanna in “Austral” showed an increase in land cover extent, which was associated
 358 with an increase in EDDI. Savanna in “Centro”, “Sur”, and “Norte Chico” decreases with the increase in
 359 EDDI. The SPI and SSI showed similar behavior regarding the trend in land cover type. A decrease in SPI
 360 and SSI is associated with an increase in the surface in shrubland and grassland in “Centro”, forest in “Sur”,
 361 and barren land in “Norte Chico”, as well as a decrease trend in savanna in “Norte Chico”, “Centro”, and
 362 “Sur”.

363 4.3. Drought impacts on vegetation productivity within land cover

364 4.3.1. Trends in vegetation productivity

365 Figure 7 shows a spatial map of trends in zcNDVI (Figure 7a). In “Norte Grande”, vegetation productivity,
 366 as per the z-index, exhibits a yearly increase of 0.027 for grassland and 0.032 for shrubland. In “Norte Chico”,
 367 savanna has the lowest trend slope of -0.062, cropland -0.047, shrubland -0.042, and grassland -0.037. In
 368 “Centro”, shrubland reaches -0.07, savanna -0.031, cropland -0.024, forest -0.017, and grassland -0.005 per
 369 decade. This decrease in productivity could be associated either with a reduction in vegetation surface, a
 370 decrease in biomass, or browning.

371 The temporal variation within the macrozones is shown in Figure 7b. There is a negative trend in “Norte
 372 Chico” with -0.035 and “Centro” with -0.02 per decade. Vegetation reached its lowest values for 2019–2022,
 373 with an extreme condition in early 2020 and 2022 in the “Norte Chico” and “Centro”. The “Sur” and
 374 “Austral” show a positive trend of around 0.012 and 0.016, respectively, per decade (Figure 7).

375 4.3.2. Correlation between vegetation productivity and drought indices

376 Figure 8 shows the time scales that reached the highest r-squared in the regression analysis between zcNDVI
 377 and different drought indicators over time scales of 1, 3, 6, 12, 24, and 36 months. The spatial variation of

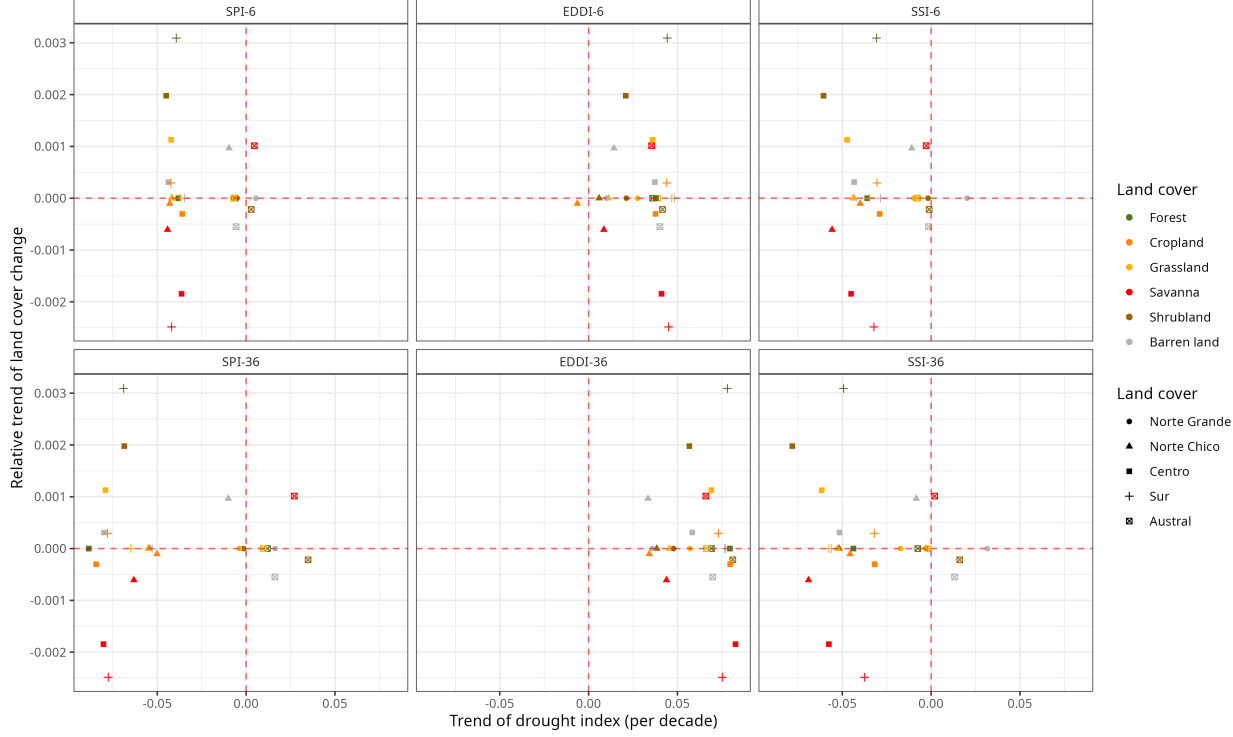


Figure 6: Relationship between the trend in land cover change (y-axis) and the trend in drought indices (x-axis) for the five macrozones. Vertical panels correspond to short (6 months) and long (36 months) time scales. Horizontal panels show the drought indices SPI, EDDI, and SSI.

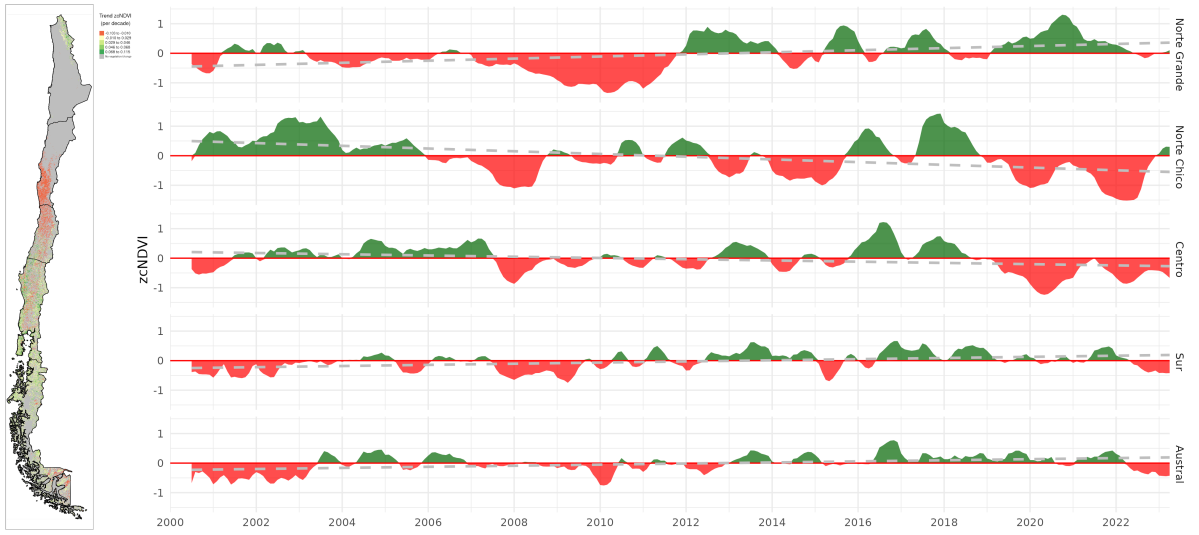


Figure 7: (a) Map of the linear trend of the index zcNDVI for 2000–2023. Greener colors indicate a positive trend; redder colors correspond to a negative trend and a decrease in vegetation productivity. Grey colors indicate either no vegetation or a change in land cover type for 2001–2022. (b) Temporal variation of zcNDVI aggregated at macrozone level within continental Chile. Each horizontal panel corresponds to a macrozone from ‘Norte Grande’ to ‘Austral’.

378 time scales reached per index is mostly for time scales above 12 months. In the case of SSI, the predominant
 379 scales are 6 and 12 months. For all indices, to the north, the time scales are higher and diminish toward the

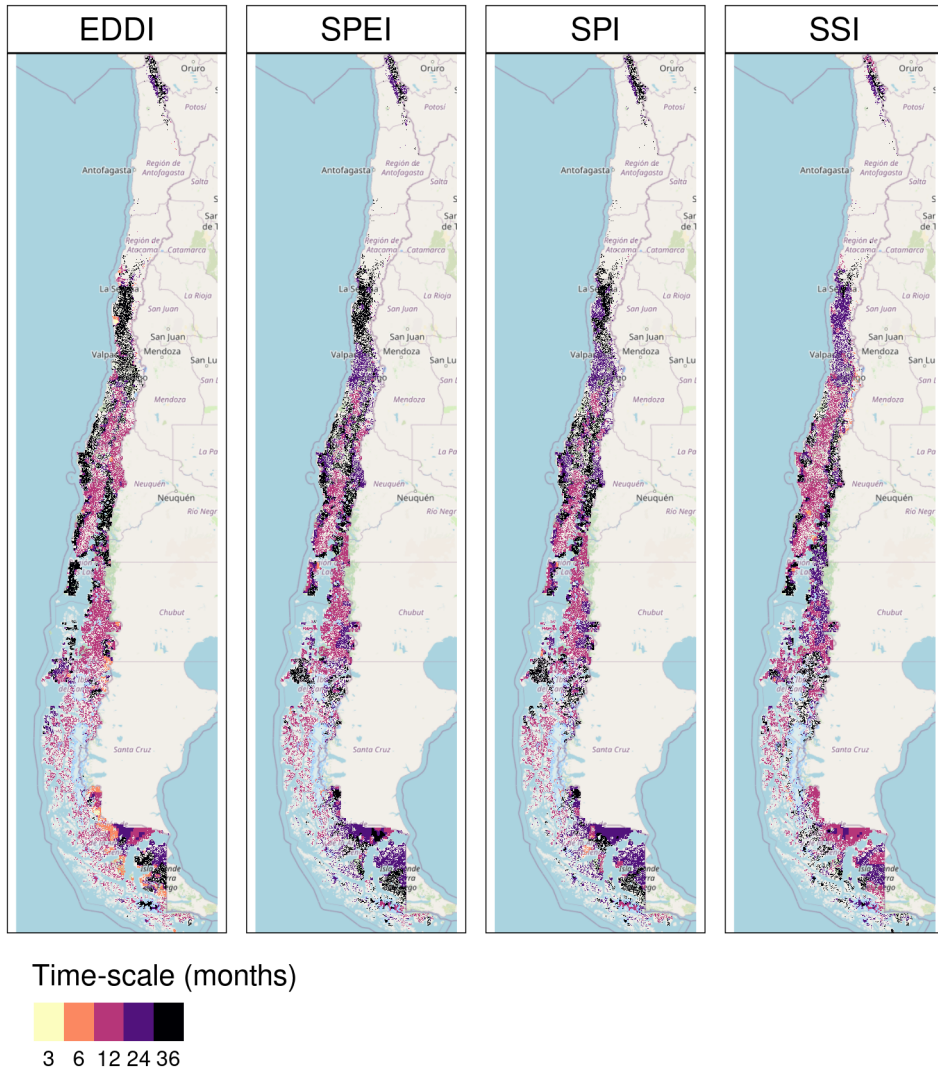


Figure 8: Time scales per drought index that reach the maximum coefficient of determination. White spaces indicate no significant correlation.

south until the south part of “Austral”, where they increase. In Figure 9, the map of Pearson correlation values (r) is shown. The EDDI reached correlations above 0.5 between “Norte Chico” and “Sur”. The correlation changes from negative to positive toward the Andes Mountains and to the sea, just as in the northern part of “Austral”. The SPI and SPEI have similar results, with the higher values in “Norte Chico” and “Centro” being higher than 0.6. Following a similar spatial pattern as EDDI but with an opposite sign. The SSI showed to be the index that has a major spatial extension with a higher correlation. It has a similar correlation to SPI and SPEI for “Norte Chico” and “Centro”, but for “Sur” the correlation is higher with SSI.

In Table 5, we aggregate per macrozone and land cover the correlation analysis presented in Figure 8 and Figure 9. According to what is shown, forests is likely to be the most resistant to drought. Showing that only “Centro” is slightly ($R^2 = 0.25$) impacted by a 12-month soil moisture deficit (SSI-12). In the “Norte Chico” and to a lesser extent in the “Norte Grande”, it is evident that a SSI-12 with a $R^2 = 0.45$ and a decrease in water supply (SPI-36 and SPEI-24 with $R^2 = 0.28$ and 0.34, respectively)

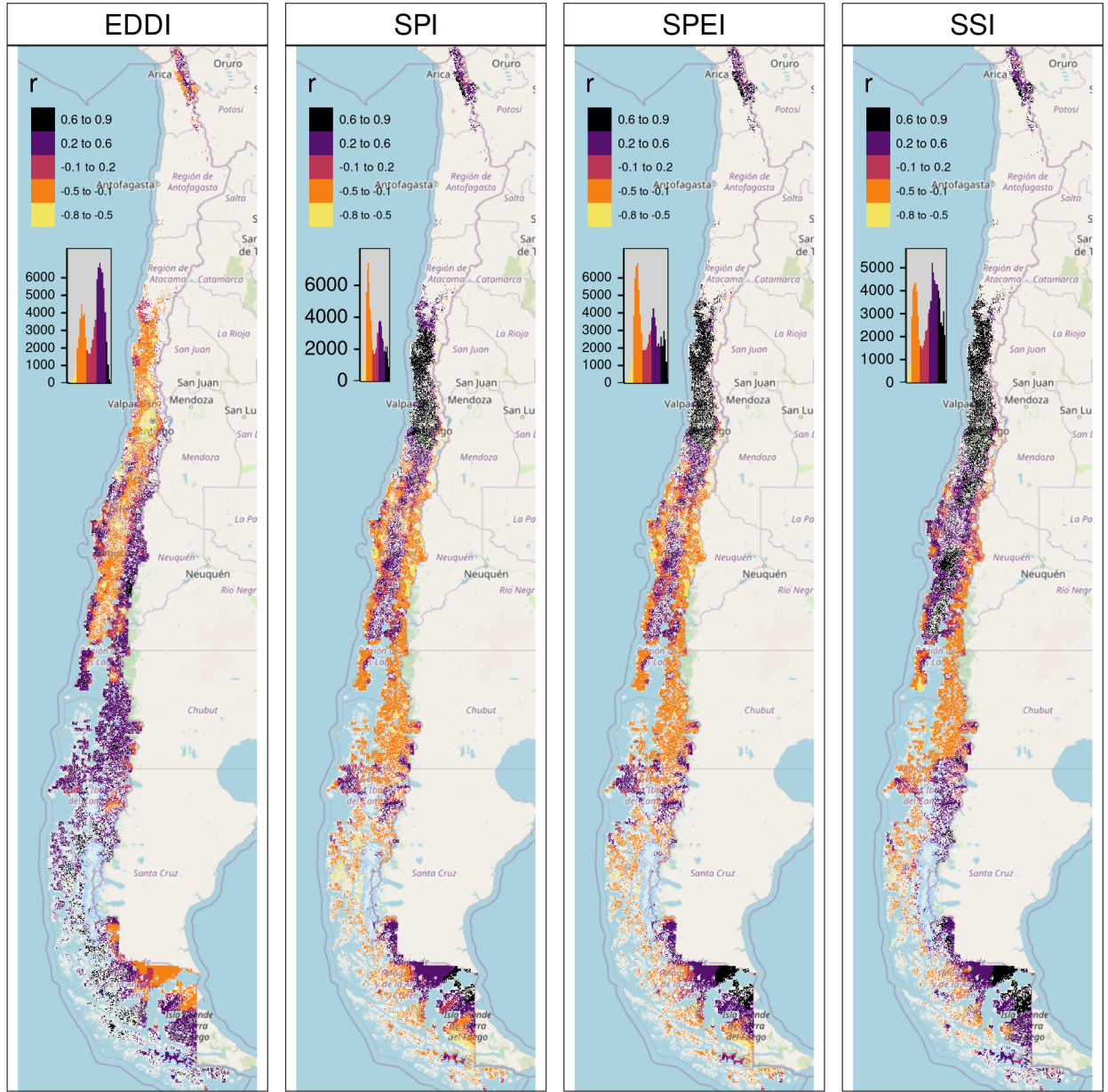


Figure 9: Pearson correlation value for the time scales and drought index that reach the maximum coefficient of determination. White spaces indicate no significant correlation.

have an impact on grasslands. However, this type was unaffected by soil moisture, water supply, or demand in macrozones further south. The types that show to be most affected by variation in climate conditions are shrublands, savannas, and croplands. For savannas in “Norte Chico”, the SSI-12 and SPI-24 reached an R^2 of 0.74 and 0.58, respectively. This value decreases to the south, but the SSI-12 is still the variable explaining more of the variation in vegetation productivity ($R^2 = 0.45$ in “Centro” and 0.2 in “Sur”). In the case of croplands, the SPEI-12, SPI-36, and SSI-12 explain between 45% and 66% of the variability in “Norte Chico”. The type of land most impacted by climatic variation was shrubland, where soil moisture explained 59% and precipitation, 37%, in “Norte Chico” and “Centro”, with SSI-12 being the most relevant variable, then SPI-36 in “Norte Chico” and SPI-24 in “Sur”.

Table 5: Summary per land cover macroclass and macrozone regarding the correlation between zcNDVI with the drought indices EDDI, SPI, SPEI, and SSI for time scales of 1, 3, 6, 12, 24, and 36. The numbers in each cell indicate the time scale that reached the maximum correlation for the land cover and macrozone, and the color indicates the strength of the r-squared obtained with the index and the time scale. Cells without values indicate that the land cover type was not significant in that macrozone.

Macrozone	Forest				Cropland				Grassland				Savanna				Shrubland			
	EDDI	SPI	SPEI	SSI	EDDI	SPI	SPEI	SSI	EDDI	SPI	SPEI	SSI	EDDI	SPI	SPEI	SSI	EDDI	SPI	SPEI	SSI
Norte Grande									36	36	36	12								
Norte Chico					36	36	12	12	36	36	24	12	36	24	24	12	36	36	24	12
Centro	36	36	12	6	12	12	6	6	12	12	12	36	12	12	12	36	24	24	12	
Sur	36					6	6	6	6	6	6	6	6	6	6	6	6			
Austral	6	6									6	12	12	6	6	12	12	6	6	6
r-squared	 0.2 0.4 0.6																			

5. Discussion

5.1. Vegetation water demand and its relation to drought

In our study, we considered the variation in vegetation productivity in Chile, specifically in areas without any changes in land cover, to prevent any misleading conclusions about the increase in water demand due to land cover change. Our results show a contrasting perspective regarding the evidence provided by [Vicente-Serrano et al. \(2022\)](#) on a global scale, who indicates that the increase in drought is led by an increase in agricultural land, which in turn increases water demand.

Our results indicate that except for the southern part of the country, the SPI, SPEI, and SSI (water supply) showed declining trends, while the EDDI (water demand) increased across continental Chile. The trends in water demand and supply were stronger as the time scales increased, indicating a long-term reduction in water supply (except for the southern part) and an increase in water demand by the atmosphere. Also, we found that there has been a significant declining trend in vegetation productivity (zcNDVI) since 2000 for the north-central part of the country, which reached its lowest level between 2020 and 2022 and has impacted natural and cultivated land. Further, croplands showed a decrease in surface area for the north-central region, while barren land increased. We link these changes to a decrease in the water demand from vegetation because, despite the increase in AED, the surface area for water-demanding vegetation is declining as well as the biomass production. However, some questions arise regarding what is occurring with the cultivated land. Evidence suggests that higher-water-demanding crops have replaced less demanding crops in the Petorca basin (central Chile), leading to an increase in water abstraction ([Muñoz et al., 2020](#); [Duran-Llacer et al., 2020](#)). Nonetheless, at this scale of analysis, the effect of higher crop water demand on drought is minor compared to the decrease in water supply and increase in AED over all land cover types.

The long-scale trends (e.g., 36 months) demonstrate the impact of climate change on water availability in Chile, potentially due to an intense hydrological drought stemming from the ongoing precipitation deficit and rising AED. But it is likely that in zones most affected by drought, the main cause is not an increase in vegetation water demand due to an intensification of cultivated land (e.g., an increase in irrigated crops) like in other parts of the globe ([Vicente-Serrano et al., 2020](#)). North-central Chile has experienced a decline in vegetation productivity across land cover types, which is primarily attributable to variations in water supply and soil moisture. An increase in water demand, led by an increase in the surface area of irrigated crops or the change to more water-demanding crops, could strengthen this trend, however, it escapes the

431 scope of this study. Future work should focus on the regions where the drought has been more severe and
432 has a high proportion of irrigated crops to get insight on the real impact of irrigation on ecosystems in those
433 zones.

434 *5.2. Sensitivity of land cover vegetation to short- and long-term drought*

435 We analyzed the time series of drought indices and vegetation productivity per land cover type. Our results
436 indicate that forest is the type most resistant to drought, and shrublands, savannas, and croplands have
437 higher sensitivities.

438 In their study in the Yangtze River Basin in China, [Jiang et al. \(2020\)](#) analyzed the impact of drought on
439 vegetation using the SPEI and the Enhanced Vegetation Index (EVI). They found that cropland was more
440 sensitive to drought than grassland, showing that cropland responds strongly to short- and medium-term
441 drought (< SPEI-6). In our case, the SPEI-12 was the one that most impacted the croplands in “Norte
442 Chico” and “Centro”. In general, most studies show that croplands are most sensitive to short-term drought
443 (< SPI-6) ([Zambrano et al., 2016](#); [Potopová et al., 2015](#); [Dai et al., 2020](#); [Rhee et al., 2010](#)). Short-term
444 precipitation deficits have an impact on soil water, so less water is available for plant growth. However, we
445 found that in “Norte Chico”, an SPI-36 and SPEI-12 had a higher impact, which are associated with long-
446 term water deficit, and in “Centro”, an SPI-12 and SPEI-12. Thus, we hypothesize that this impact could
447 be attributed to the hydrological drought that has decreased groundwater storage ([Tau care et al., 2024](#)),
448 which in turn is impacted by long-term deficits, and consequently, the vegetation is more dependent on
449 groundwater. In “Sur” and “Austral”, the correlations between drought indices and vegetation productivity
450 decrease, as do the time scales that reach the maximum r-squared. The possible reason for this is that the
451 most resistant types, forest and grassland, predominate south of “Centro”. Also, drought episodes have been
452 less frequent and intense and have had a lower impact on water availability for vegetation.

453 In central Chile, [Venegas-González et al. \(2023\)](#) observed a significant decline in the overall growth of
454 sclerophyllous moist forests (mediterranean forests), which they attributed to increased drought conditions.
455 However, we found that forests are the most resilient land cover class to drought, with less variation in
456 drought indices. In the “Sur”, there is a large domain of planted forests that have replaced native vegetation
457 since the 1970s ([Heilmayr et al., 2016, 2020](#); [Miranda et al., 2017](#)), impacting biodiversity and ecosystem
458 services ([Rodríguez-Echeverry et al., 2018](#)). It has recently been shown that these planted forests are
459 responding positively to climate change, and it is expected that they will benefit from future climate scenarios
460 ([Carrasco et al., 2022](#)). Further, the forests of the “Austral” region correspond to Patagonian ecosystems,
461 mainly native forests dominated by tree species of wide niche breadth . Overall, these forests have been
462 more affected by the increase in temperature than by the reduction in moisture ([Fajardo et al., 2023](#); [Holz
et al., 2018](#)). These responses have caused stabilized tree growth, linked to more frequent warm autumns
463 ([Gibson-Carpintero et al., 2022](#)). It has also been observed that these forests have shown resistance to
464 drought episodes ([Fajardo et al., 2023](#)), which might be attributable to their relatively low growth rate.
465 Supporting this is [Fathi-Taperasht et al. \(2022\)](#), who assert that Indian forests are the most drought-
466 resistant and recover rapidly. Similarly, the work of [Wu et al. \(2024\)](#), who analyzed vegetation loss and
467 recovery in response to meteorological drought in the humid subtropical Pearl River basin in China, indicates
468 that forests showed higher drought resistance. Using Vegetation Optical Depth (VOD), kNDVI, and EVI,
469 [Xiao et al. \(2023\)](#) tested the resistance of ecosystems and found that ecosystems with more forests are better
470 able to handle severe droughts than croplands. They attribute the difference to a deeper rooting depth for
471 trees, a higher water storage capacity, and different water use strategies between forest and cropland ([Xiao
et al., 2023](#)).

474 In another study, [Fuentes et al. \(2021\)](#) evaluated water scarcity and land cover change in Chile between 29°
475 and 39° south latitude. They used the one-month SPEI for drought evaluation, which resulted in misleading
476 results. For instance, they failed to identify a temporal trend in the SPEI, but they still observed a decline
477 in water availability and a rise in AED, trends that should have been detectable if they were using longer
478 SPEI time scales. Thus, according to the results presented in this study, for the assessment of drought, it is
479 necessary to consider drought indices on a short- to long-scale basis.

480 5.3. Vegetation productivity and drought

481 We found that the 12-month soil moisture deficit affected plant productivity in all land cover types in
482 Chile. The main external factors that affect biomass production by vegetation are actual evapotranspiration
483 and soil moisture, and the rate of ET in turn depends on the availability of water storage in the root zone.
484 Thus, soil moisture plays a key role in land carbon uptake and, consequently, in the production of biomass
485 ([Humphrey et al., 2021](#)). The study results showed that the soil moisture-based drought index (SSI) was
486 better at explaining vegetation productivity across land cover macroclasses than meteorological drought
487 indices like SPI, SPEI, and EDDI. According to ([Chatterjee et al., 2022](#)) in the early growing season and
488 especially in irrigated rather than rainfed croplands, soil moisture has better skills than SPI and SPEI
489 for estimating gross primary production (GPP). Also, [Zhou et al. \(2021\)](#) indicate that the monthly scaled
490 Standardized Water Deficit Index (SWDI) can accurately show the effects of agricultural drought in most
491 of China. [Nicolai-Shaw et al. \(2017\)](#) also looked at the time-lag between the SWDI and the Vegetation
492 Condition Index (VCI). They found that there was little to no time-lag in croplands but a greater time-lag
493 in forests.

494 In our case, there is strong spatial variability throughout Chile and between classes, mainly attributable to
495 climate heterogeneity, hydrological status, or vegetation resistance to water scarcity. The semi-arid “Norte
496 Chico” and the Mediterranean “Centro” were where SSI had the best performance. In Chile, medium-
497 term deficits of 12 months are more relevant in the response of vegetation for all land cover types, which
498 decreases to the south, and in the case of croplands, they seem to react in a shorter time, with six months
499 (SSI-6) in “Centro”. This variation for croplands could be related to the fact that in “Norte Chico”, the
500 majority of crops are irrigated, but to the south there is a higher proportion of rainfed agriculture, which
501 is most dependent on the short-term availability of water. Rather, in “Norte Chico”, the orchards are more
502 dependent on irrigation, which in turn depends on the availability of storage water in dams or groundwater
503 reservoirs, which are affected by long-term drought (e.g., SPI-36).

504 5.4. Drought information to aid in adaptation

505 Our findings present valuable information for policymakers in developing adaptation strategies for droughts.
506 Our results show that the different climate components, such as AED, water supply, soil moisture, and their
507 impact on vegetation, should be considered when evaluating the multi-dimensional nature of drought. Also,
508 for a better understanding of drought propagation ([Van Loon et al., 2012](#)) from meteorological to agricultural
509 and ecological drought, we should consider the climatic response at different time scales, ranging from short
510 to long. Additionally, the spatiotemporal characteristics of our results allow us to distinguish distinct
511 geographical contexts, recognizing the diversity in climate, but also shedding light on agricultural practices
512 (ranging from irrigated to dryland farming), technological advancements in irrigation efficiency, and the
513 region-specific capabilities for drought adaptation, including groundwater management and reservoir water
514 storage. This information, combined with agricultural information and statistics, could provide a strong
515 foundation for the development of science-based adaptation policies.

516 In a commitment to fostering informed and dynamic adaptation efforts, our results are disseminated
517 publicly and continually updated via the Drought Observatory for Agriculture and Biodiversity of Chile
518 (ODES) <https://odes-chile.org/app/unidades> ([Zambrano, 2023a; Kunst and Zambrano, 2023](#)). This initiative
519 ensures the availability and easy accessibility of extensive climate data, facilitating the development
520 of adaptive strategies that are both responsive to the realities of different regions and grounded in the lat-
521 est scientific understanding. The proactive sharing and updating of such data underscores its key role in
522 enabling policymakers to craft adaptive measures that are finely tuned to the diverse and evolving land-
523 scapes of drought impacts. Furthermore, the recently promulgated law about climate change in Chile (Law
524 21.455, <https://www.bcn.cl/leychile/navegar?idNorma=1177286>), which aims to implement sectoral adap-
525 tation plans for agriculture, forests, and biodiversity, could benefit from this information.

526 **6. Conclusion**

527 We found a significant trend toward decreasing water supply (SPI, SPEI, and SSI) in most of the Chilean
528 territory, with the exception of the southern region. The trend is the strongest in the north-central zone. The
529 whole country showed an increase in water demand (AED) due to increasing temperatures. The magnitude
530 of the trends is stronger for longer time scales, which is evidence that there is a prolonged precipitation
531 shortage and a prolonged increase in AED. The trend in vegetation productivity in the north-central area
532 is affecting shrubland and savanna to a greater degree, followed by croplands and forests.

533 Using Random Forest and variable importance metrics, we assessed how land cover trends relate to drought
534 indices and found that drought indices across Chile could explain about 12–41% of the trends in land cover
535 types. Drought explains a higher variance in changes in shrublands, followed by savanna, grasslands, and
536 forest. The changes in croplands showed the lowest association with drought. We found that the short- to
537 long-term trend in AED was the most important variable that could partially explain the observed land
538 cover trend, followed by long-term trends in precipitation and short-term trends in soil moisture.

539 The trends in drought indices are accompanied by multiple land cover changes in the country, most notably
540 an increase of forest in “Sur”, of shrubland and grassland in “Centro”, and of savanna in “Centro” and “Sur”.
541 In “Norte Chico” and “Centro”, the croplands have been declining in surface, whereas in “Sur”, there is an
542 increase in cultivated land.

543 The change in vegetation productivity has been severe in the north-central part of the country for all land
544 cover types, particularly savanna, shrubland, and croplands. The anomaly in soil moisture over the past 12
545 months is the main variable explaining these changes, followed by anomalies in accumulated precipitation
546 over one to two years. The variation in AED is likely to exacerbate the drought’s impact on vegetation
547 productivity.

548 The results of this study provide insightful information that can assist in developing adaptation measures
549 for Chilean ecosystems to cope with climate change and drought. This information could be used in the
550 scope of the national law on climate change, which seeks to implement adaptation strategies for agriculture,
551 forests, and biodiversity.

552 **7. Acknowledgment**

553 The National Research and Development Agency of Chile (ANID) funded this study through the drought
554 emergency project FSEQ210022, Fondecyt Iniciación N°11190360, Fondecyt Postdoctorado N°3230678, and
555 Fondecyt Regular N°1210526. The companies Garces Fruit and CER Analytics provided access to the *in-situ*
556 soil moisture data used in this work.

557 **References**

- 558 Abramowitz, M., Stegun, I.A., 1968. Handbook of mathematical functions with formulas, graphs, and mathematical tables.
559 volume 55. US Government printing office.
560 Aceituno, P., Boisier, J.P., Garreaud, R., Rondanelli, R., Ruttlant, J.A., 2021. Climate and Weather in Chile, in: Fernández,
561 B., Gironás, J. (Eds.), Water Resources of Chile. Springer International Publishing, Cham. volume 8, pp. 7–29. URL:
562 http://link.springer.com/10.1007/978-3-030-56901-3_2.
563 AghaKouchak, A., 2014. A baseline probabilistic drought forecasting framework using standardized soil moisture in-
564 dex: application to the 2012 United States drought. Hydrology and Earth System Sciences 18, 2485–2492. URL:
565 <https://hess.copernicus.org/articles/18/2485/2014/>, doi:10.5194/hess-18-2485-2014.
566 AghaKouchak, A., Mirchi, A., Madani, K., Di Baldassarre, G., Nazemi, A., Alborzi, A., Anjileli, H., Azarderakhsh, M., Chiang,
567 F., Hassanzadeh, E., Huning, L.S., Mallakpour, I., Martinez, A., Mazdiyasni, O., Moftakhari, H., Norouzi, H., Sadegh,
568 M., Sadeqi, D., Van Loon, A.F., Wanders, N., 2021. Anthropogenic Drought: Definition, Challenges, and Opportunities.
569 Reviews of Geophysics 59, e2019RG000683. URL: <https://agupubs.onlinelibrary.wiley.com/doi/10.1029/2019RG000683>,
570 doi:10.1029/2019RG000683.

- 571 Akinyemi, F.O., 2021. Vegetation Trends, Drought Severity and Land Use-Land Cover Change during the Growing Season in
 572 Semi-Arid Contexts. *Remote Sensing* 2021, Vol. 13, Page 836 13, 836. URL: <https://www.mdpi.com/2072-4292/13/5/836/htm>, doi:[10.3390/RS13050836](https://doi.org/10.3390/RS13050836). publisher: Multidisciplinary Digital Publishing Institute.
- 573 Alvarez-Garreton, C., Boisier, J.P., Garreaud, R., Seibert, J., Vis, M., 2021. Progressive water deficits during multiyear
 574 droughts in basins with long hydrological memory in Chile. *Hydrology and Earth System Sciences* 25, 429–446. URL:
 575 <https://hess.copernicus.org/articles/25/429/2021/>, doi:[10.5194/hess-25-429-2021](https://doi.org/10.5194/hess-25-429-2021).
- 576 Bakker, K., 2012. Water Security: Research Challenges and Opportunities. *Science* 337, 914–915. URL: <https://www.science.org/doi/10.1126/science.1226337>, doi:[10.1126/science.1226337](https://doi.org/10.1126/science.1226337).
- 577 Barría, P., Sandoval, I.B., Guzman, C., Chadwick, C., Alvarez-Garreton, C., Díaz-Vasconcellos, R., Ocampo-Melgar,
 578 A., Fuster, R., 2021. Water allocation under climate change. *Elementa: Science of the Anthropocene* 9,
 579 00131. URL: <https://online.ucpress.edu/elementa/article/9/1/00131/117183/Water-allocation-under-climate-changeA-diagnosis>, doi:[10.1525/elementa.2020.00131](https://doi.org/10.1525/elementa.2020.00131).
- 580 Beck, H.E., McVicar, T.R., Vergopolan, N., Berg, A., Lutsko, N.J., Dufour, A., Zeng, Z., Jiang, X., van Dijk, A.I.J.M., Miralles,
 581 D.G., 2023. High-resolution (1 km) Köppen-Geiger maps for 1901–2099 based on constrained CMIP6 projections. *Scientific
 582 Data* 10. URL: <http://dx.doi.org/10.1038/s41597-023-02549-6>, doi:[10.1038/s41597-023-02549-6](https://doi.org/10.1038/s41597-023-02549-6).
- 583 Beguería, S., Vicente-Serrano, S.M., 2023. SPEI: Calculation of the Standardized Precipitation-Evapotranspiration Index.
 584 URL: <https://CRAN.R-project.org/package=SPEI>.
- 585 Boisier, J.P., Alvarez-Garreton, C., Cordero, R.R., Damiani, A., Gallardo, L., Garreaud, R.D., Lambert, F., Ramallo, C.,
 586 Rojas, M., Rondanelli, R., 2018. Anthropogenic drying in central-southern Chile evidenced by long-term observations
 587 and climate model simulations. *Elementa* 6, 74. URL: <https://www.elementascience.org/article/10.1525/elementa.328/>,
 588 doi:[10.1525/elementa.328](https://doi.org/10.1525/elementa.328).
- 589 Calvin, K., Dasgupta, D., Krinner, G., Mukherji, A., Thorne, P.W., Trisos, C., Romero, J., Aldunce, P., Barrett, K., Blanco,
 590 G., Cheung, W.W., Connors, S., Denton, F., Diongue-Niang, A., Dodman, D., Garschagen, M., Geden, O., Hayward, B.,
 591 Jones, C., Jotzo, F., Krug, T., Lasco, R., Lee, Y.Y., Masson-Delmotte, V., Meinshausen, M., Mintenbeck, K., Mokssit, A.,
 592 Otto, F.E., Pathak, M., Pirani, A., Poloczanska, E., Pörtner, H.O., Revi, A., Roberts, D.C., Roy, J., Ruane, A.C., Skea,
 593 J., Shukla, P.R., Slade, R., Slangen, A., Sokona, Y., Sörensson, A.A., Tignor, M., Van Vuuren, D., Wei, Y.M., Winkler,
 594 H., Zhai, P., Zommers, Z., Hourcade, J.C., Johnson, F.X., Pachauri, S., Simpson, N.P., Singh, C., Thomas, A., Totin, E.,
 595 Arias, P., Bustamante, M., Elgizouli, I., Flato, G., Howden, M., Méndez-Vallejo, C., Pereira, J.J., Pichs-Madruga, R., Rose,
 596 S.K., Saheb, Y., Sánchez Rodríguez, R., Ürge Vorsatz, D., Xiao, C., Yassaa, N., Alegría, A., Armour, K., Bednar-Friedl, B.,
 597 Blok, K., Cissé, G., Dentener, F., Eriksen, S., Fischer, E., Garner, G., Guiavarch, C., Haasnoot, M., Hansen, G., Hauser, M.,
 598 Hawkins, E., Hermans, T., Kopp, R., Leprince-Ringuet, N., Lewis, J., Ley, D., Ludden, C., Niamir, L., Nicholls, Z., Some,
 599 S., Szopa, S., Trewin, B., Van Der Wijst, K.I., Winter, G., Witting, M., Birt, A., Ha, M., Romero, J., Kim, J., Haites, E.F.,
 600 Jung, Y., Stavins, R., Birt, A., Ha, M., Orendain, D.J.A., Ignon, L., Park, S., Park, Y., Reisinger, A., Cammaramo, D.,
 601 Fischlin, A., Fuglestvedt, J.S., Hansen, G., Ludden, C., Masson-Delmotte, V., Matthews, J.R., Mintenbeck, K., Pirani, A.,
 602 Poloczanska, E., Leprince-Ringuet, N., Péan, C., 2023. IPCC, 2023: Climate Change 2023: Synthesis Report. Contribution
 603 of Working Groups I, II and III to the Sixth Assessment Report of the Intergovernmental Panel on Climate Change [Core
 604 Writing Team, H. Lee and J. Romero (eds.)]. IPCC, Geneva, Switzerland. Technical Report. Intergovernmental Panel on
 605 Climate Change (IPCC). URL: <https://www.ipcc.ch/report/ar6/syr/>.
- 606 Camps-Valls, G., Campos-Taberner, M., Moreno-Martínez, ., Walther, S., Duveiller, G., Cescatti, A., Mahecha, M.D., Muñoz-
 607 Marí, J., García-Haro, F.J., Guanter, L., Jung, M., Gamon, J.A., Reichstein, M., Running, S.W., 2021. A unified vegetation
 608 index for quantifying the terrestrial biosphere. *Science Advances* 7, eabc7447. URL: <https://www.science.org/doi/10.1126/sciadv.abc7447>, doi:[10.1126/sciadv.abc7447](https://doi.org/10.1126/sciadv.abc7447).
- 609 Carrasco, G., Almeida, A.C., Falvey, M., Olmedo, G.F., Taylor, P., Santibañez, F., Coops, N.C., 2022. Effects of climate change
 610 on forest plantation productivity in Chile. *Global Change Biology* 28, 7391–7409. URL: <https://onlinelibrary.wiley.com/doi/10.1111/gcb.16418>, doi:[10.1111/gcb.16418](https://doi.org/10.1111/gcb.16418).
- 611 Chamling, M., Bera, B., 2020. Spatio-temporal Patterns of Land Use/Land Cover Change in the Bhutan–Bengal Foothill Region
 612 Between 1987 and 2019: Study Towards Geospatial Applications and Policy Making. *Earth Systems and Environment* 4,
 613 117–130. URL: <http://link.springer.com/10.1007/s41748-020-00150-0>, doi:[10.1007/s41748-020-00150-0](https://doi.org/10.1007/s41748-020-00150-0).
- 614 Chatterjee, S., Desai, A.R., Zhu, J., Townsend, P.A., Huang, J., 2022. Soil moisture as an essential component for delineating
 615 and forecasting agricultural rather than meteorological drought. *Remote Sensing of Environment* 269, 112833. URL:
 616 <https://linkinghub.elsevier.com/retrieve/pii/S0034425721005538>, doi:[10.1016/j.rse.2021.112833](https://doi.org/10.1016/j.rse.2021.112833).
- 617 Chen, J., Shao, Z., Huang, X., Zhuang, Q., Dang, C., Cai, B., Zheng, X., Ding, Q., 2022. Assessing the impact of drought-
 618 land cover change on global vegetation greenness and productivity. *Science of The Total Environment* 852, 158499. URL:
 619 <https://linkinghub.elsevier.com/retrieve/pii/S004896972205598X>, doi:[10.1016/j.scitotenv.2022.158499](https://doi.org/10.1016/j.scitotenv.2022.158499).
- 620 Cheng, Y., Oehmcke, S., Brandt, M., Rosenthal, L., Das, A., Vrieling, A., Saatchi, S., Wagner, F., Mugabowindekwe, M.,
 621 Verbruggen, W., Beier, C., Horion, S., 2024. Scattered tree death contributes to substantial forest loss in California. *Nature
 622 Communications* 15, 641. URL: <https://www.nature.com/articles/s41467-024-44991-z>, doi:[10.1038/s41467-024-44991-z](https://doi.org/10.1038/s41467-024-44991-z).
- 623 Crausbay, S.D., Ramirez, A.R., Carter, S.L., Cross, M.S., Hall, K.R., Bathke, D.J., Betancourt, J.L., Colt, S., Cravens, A.E.,
 624 Dalton, M.S., Dunham, J.B., Hay, L.E., Hayes, M.J., McEvoy, J., McNutt, C.A., Moritz, M.A., Nislow, K.H., Raheem, N.,
 625 Sanford, T., 2017. Defining Ecological Drought for the Twenty-First Century. *Bulletin of the American Meteorological Society*
 626 98, 2543–2550. URL: <https://journals.ametsoc.org/view/journals/bams/98/12/bams-d-16-0292.1.xml>, doi:[10.1175/BAMS-D-16-0292.1](https://doi.org/10.1175/BAMS-D-16-0292.1). publisher: American Meteorological Society.
- 627 Dai, M., Huang, S., Huang, Q., Leng, G., Guo, Y., Wang, L., Fang, W., Li, P., Zheng, X., 2020. Assessing agricultural drought
 628 risk and its dynamic evolution characteristics. *Agricultural Water Management* 231, 106003. URL: [https://linkinghub.elsevier.com/retrieve/pii/S0378377419316531](https://linkinghub.

 629 elsevier.com/retrieve/pii/S0378377419316531), doi:[10.1016/j.agwat.2020.106003](https://doi.org/10.1016/j.agwat.2020.106003).

- 636 Didan, K., 2015. MOD13Q1 MODIS/Terra Vegetation Indices 16-Day L3 Global 250m SIN Grid V006. Technical Report.
 637 NASA EOSDIS Land Processes DAAC. doi:<http://dx.doi.org/10.5067/MODIS/MOD13Q1.006>.
- 638 Duran-Llacer, I., Munizaga, J., Arumí, J., Ruybal, C., Aguayo, M., Sáez-Carrillo, K., Arriagada, L., Rojas, O., 2020. Lessons
 639 to Be Learned: Groundwater Depletion in Chile's Ligua and Petorca Watersheds through an Interdisciplinary Approach.
 640 Water 12, 2446. URL: <https://www.mdpi.com/2073-4441/12/9/2446>, doi:10.3390/w12092446.
- 641 Echeverría, C., Newton, A., Nahuelhual, L., Coomes, D., Rey-Benayas, J.M., 2012. How landscapes change: Integration of
 642 spatial patterns and human processes in temperate landscapes of southern Chile. Applied Geography 32, 822–831. URL:
 643 <https://linkinghub.elsevier.com/retrieve/pii/S0143622811001676>, doi:10.1016/j.apgeog.2011.08.014.
- 644 Fajardo, A., Gazol, A., Meynard, P.M., Mayr, C., Martínez Pastur, G.J., Peri, P.L., Camarero, J.J., 2023. Climate change-
 645 related growth improvements in a wide niche-breadth tree species across contrasting environments. Annals of Botany 131,
 646 941–951. URL: <https://academic.oup.com/aob/article/131/6/941/7095679>, doi:10.1093/aob/mcad053.
- 647 FAO, 2022. The State of the World's Forests 2022. FAO. URL: <http://www.fao.org/documents/card/en/c/cb9360en>.
- 648 Farahmand, A., AghaKouchak, A., 2015. A generalized framework for deriving nonparametric standardized drought indicators.
 649 Advances in Water Resources 76, 140–145. URL: <https://linkinghub.elsevier.com/retrieve/pii/S0309170814002322>, doi:10.
 650 1016/j.advwatres.2014.11.012.
- 651 Fathi-Taperasht, A., Shafizadeh-Moghadam, H., Minaei, M., Xu, T., 2022. Influence of drought duration and severity on
 652 drought recovery period for different land cover types: evaluation using MODIS-based indices. Ecological Indicators 141,
 653 109146. URL: <https://linkinghub.elsevier.com/retrieve/pii/S1470160X22006185>, doi:10.1016/j.ecolind.2022.109146.
- 654 Ford, T.W., Otkin, J.A., Quiring, S.M., Lisonbee, J., Woloszyn, M., Wang, J., Zhong, Y., 2023. Flash Drought Indicator
 655 Intercomparison in the United States. Journal of Applied Meteorology and Climatology 62, 1713–1730. URL: <https://journals.ametsoc.org/view/journals/apme/62/12/JAMC-D-23-0081.1.xml>, doi:10.1175/JAMC-D-23-0081.1.
- 656 Fuentes, I., Fuster, R., Avilés, D., Vervoort, W., 2021. Water scarcity in central Chile: the effect of climate and land cover
 657 changes on hydrologic resources. Hydrological Sciences Journal 66, 1028–1044. URL: <https://www.tandfonline.com/doi/full/10.1080/02626667.2021.1903475>, doi:10.1080/02626667.2021.1903475.
- 658 Garreaud, R., Alvarez-Garreton, C., Barichivich, J., Boisier, J.P., Christie, D., Galleguillos, M., LeQuesne, C., McPhee,
 659 J., Zambrano-Bigiarini, M., 2017. The 2010–2015 mega drought in Central Chile: Impacts on regional hydroclimate and
 660 vegetation. Hydrology and Earth System Sciences Discussions 2017, 1–37. URL: <http://www.hydrol-earth-syst-sci-discuss.net/hess-2017-191/>, doi:10.5194/hess-2017-191.
- 661 Garreaud, R.D., 2009. The Andes climate and weather. Advances in Geosciences 22, 3–11. URL: <https://adgeo.copernicus.org/articles/22/3/2009/>, doi:10.5194/adgeo-22-3-2009.
- 662 Gebrechorkos, S.H., Peng, J., Dyer, E., Miralles, D.G., Vicente-Serrano, S.M., Funk, C., Beck, H.E., Asfaw, D.T., Singer, M.B.,
 663 Dadson, S.J., 2023. Global high-resolution drought indices for 1981–2022. Earth System Science Data 15, 5449–5466. URL:
 664 <https://essd.copernicus.org/articles/15/5449/2023/>, doi:10.5194/essd-15-5449-2023.
- 665 Gibson-Carpintero, S., Venegas-González, A., Urra, V.D., Estay, S.A., Gutiérrez, .G., 2022. Recent increase in autumn
 666 temperature has stabilized tree growth in forests near the tree lines in Chilean Patagonia. Ecosphere 13, e4266. URL:
 667 <https://esajournals.onlinelibrary.wiley.com/doi/10.1002/ecs2.4266>, doi:10.1002/ecs2.4266.
- 668 Hao, Z., AghaKouchak, A., 2013. Multivariate Standardized Drought Index: A parametric multi-index model. Advances in Water-
 669 ter Resources 57, 12–18. URL: <https://linkinghub.elsevier.com/retrieve/pii/S0309170813000493>, doi:10.1016/j.advwatres.2013.03.009.
- 670 Hargreaves, G.H., 1994. Defining and Using Reference Evapotranspiration. Journal of Irrigation and Drainage Engineering 120,
 671 1132–1139. URL: <https://ascelibrary.org/doi/10.1061/%28ASCE%290733-9437%281994%29120%3A6%281132%29>, doi:10.
 672 1061/(ASCE)0733-9437(1994)120:6(1132).
- 673 Hargreaves, G.H., Samani, Z.A., 1985. Reference crop evapotranspiration from temperature. Applied engineering in agriculture
 674 1, 96–99.
- 675 Heilmayr, R., Echeverría, C., Fuentes, R., Lambin, E.F., 2016. A plantation-dominated forest transition in Chile. Applied
 676 Geography 75, 71–82. URL: <https://linkinghub.elsevier.com/retrieve/pii/S0143622816302600>, doi:10.1016/j.apgeog.2016.07.014.
- 677 Heilmayr, R., Echeverría, C., Lambin, E.F., 2020. Impacts of Chilean forest subsidies on forest cover, carbon and biodiversity.
 678 Nature Sustainability 3, 701–709. URL: <https://www.nature.com/articles/s41893-020-0547-0>.
- 679 Heim, R.R., 2002. A Review of Twentieth-Century Drought Indices Used in the United States. Bulletin of the American
 680 Meteorological Society 83, 1149–1166. URL: <https://journals.ametsoc.org/doi/10.1175/1520-0477-83.8.1149>, doi:10.1175/
 681 1520-0477-83.8.1149.
- 682 Helman, D., Mussery, A., Lensky, I.M., Leu, S., 2014. Detecting changes in biomass productivity in a different land management
 683 regimes in drylands using satellite-derived vegetation index. Soil Use and Management 30, 32–39. URL: <https://bsssjournals.onlinelibrary.wiley.com/doi/10.1111/sum.12099>, doi:10.1111/sum.12099.
- 684 Hijmans, R.J., 2023. terra: Spatial Data Analysis. URL: <https://CRAN.R-project.org/package=terra>.
- 685 Ho, T.K., 1995. Random decision forests, in: Proceedings of 3rd international conference on document analysis and recognition,
 686 IEEE. pp. 278–282.
- 687 Hobbins, M.T., Wood, A., McEvoy, D.J., Huntington, J.L., Morton, C., Anderson, M., Hain, C., 2016. The Evaporative Demand
 688 Drought Index. Part I: Linking Drought Evolution to Variations in Evaporative Demand. Journal of Hydrometeorology 17,
 689 1745–1761. URL: <http://journals.ametsoc.org/doi/10.1175/JHM-D-15-0121.1>, doi:10.1175/JHM-D-15-0121.1.
- 690 Holz, A., Hart, S.J., Williamson, G.J., Veblen, T.T., Aravena, J.C., 2018. Radial growth response to climate change along the
 691 latitudinal range of the world's southernmost conifer in southern South America. Journal of Biogeography 45, 1140–1152.
 692 URL: <https://onlinelibrary.wiley.com/doi/10.1111/jbi.13199>, doi:10.1111/jbi.13199.

- 701 Homer, C., Dewitz, J., Jin, S., Xian, G., Costello, C., Danielson, P., Gass, L., Funk, M., Wickham, J., Stehman, S., Auch, R.,
 702 Riitters, K., 2020. Conterminous United States land cover change patterns 2001–2016 from the 2016 National Land Cover
 703 Database. *ISPRS Journal of Photogrammetry and Remote Sensing* 162, 184–199. URL: <https://linkinghub.elsevier.com/retrieve/pii/S0924271620300587>, doi:10.1016/j.isprsjprs.2020.02.019.
- 704 Hufkens, K., Staufer, R., Campitelli, E., 2019. The ecwmfr package: an interface to ECMWF API endpoints. URL: <https://bluegreen-labs.github.io/ecmwfr/>.
- 705 Humphrey, V., Berg, A., Ciais, P., Gentine, P., Jung, M., Reichstein, M., Seneviratne, S.I., Frankenberg, C., 2021. Soil
 706 moisture–atmosphere feedback dominates land carbon uptake variability. *Nature* 592, 65–69. URL: <https://www.nature.com/articles/s41586-021-03325-5>, doi:10.1038/s41586-021-03325-5.
- 707 IPCC, 2013. Climate Change 2013: The Physical Science Basis. Contribution of Working Group I to the Fifth Assessment
 708 Report of the Intergovernmental Panel on Climate Change. Cambridge University Press, Cambridge, UK; New York, USA.
 709 URL: www.climatechange2013.org, doi:10.1017/CBO9781107415324.
- 710 Jiang, W., Wang, L., Feng, L., Zhang, M., Yao, R., 2020. Drought characteristics and its impact on changes in surface
 711 vegetation from 1981 to 2015 in the Yangtze River Basin, China. *International Journal of Climatology* 40, 3380–3397. URL:
 712 <https://rmets.onlinelibrary.wiley.com/doi/10.1002/joc.6403>, doi:10.1002/joc.6403.
- 713 Kendall, M., 1975. Rank correlation methods (4th ed. 2d impression). Griffin.
- 714 Kogan, F., Guo, W., Yang, W., 2020. Near 40-year drought trend during 1981–2019 earth warming and food security. *Geomatics, Natural Hazards and Risk* 11, 469–490. URL: <https://www.tandfonline.com/doi/full/10.1080/19475705.2020.1730452>, doi:10.1080/19475705.2020.1730452.
- 715 Kuhn, M., Wickham, H., 2020. Tidymodels: a collection of packages for modeling and machine learning using tidyverse
 716 principles. URL: <https://www.tidymodels.org>.
- 717 Kunst, J., Zambrano, F., 2023. ODES Estaciones. URL: <https://zenodo.org/record/8189816>.
- 718 Laimighofer, J., Laaha, G., 2022. How standard are standardized drought indices? Uncertainty components for the SPI
 719 & SPEI case. *Journal of Hydrology* 613, 128385. URL: <https://linkinghub.elsevier.com/retrieve/pii/S0022169422009544>, doi:10.1016/j.jhydrol.2022.128385.
- 720 Li, H., Choy, S., Zaminpardaz, S., Wang, X., Liang, H., Zhang, K., 2024. Flash drought monitoring using diurnal-provided
 721 evaporative demand drought index. *Journal of Hydrology* 633, 130961. URL: <https://linkinghub.elsevier.com/retrieve/pii/S002216942400355X>, doi:10.1016/j.jhydrol.2024.130961.
- 722 Li, W., Migliavacca, M., Forkel, M., Denissen, J.M.C., Reichstein, M., Yang, H., Duveiller, G., Weber, U., Orth, R., 2022.
 723 Widespread increasing vegetation sensitivity to soil moisture. *Nature Communications* 13, 3959. URL: <https://www.nature.com/articles/s41467-022-31667-9>, doi:10.1038/s41467-022-31667-9.
- 724 Liu, X., Yu, S., Yang, Z., Dong, J., Peng, J., 2024. The first global multi-timescale daily SPEI dataset from 1982 to 2021.
 725 Scientific Data 11, 223. URL: <https://www.nature.com/articles/s41597-024-03047-z>, doi:10.1038/s41597-024-03047-z.
- 726 Luebert, F., Pliscoff, P., 2022. The vegetation of Chile and the EcoVeg approach in the context of the International Vegetation
 727 Classification project. *Vegetation Classification and Survey* 3, 15–28. URL: <https://vcs.pensoft.net/article/67893/>, doi:10.3897/VCS.67893.
- 728 Luyssaert, S., Jammet, M., Stoy, P.C., Estel, S., Pongratz, J., Ceschia, E., Churkina, G., Don, A., Erb, K., Ferlicq, M.,
 729 Gielen, B., Grünwald, T., Houghton, R.A., Klumpp, K., Knohl, A., Kolb, T., Kuemmerle, T., Laurila, T., Lohila, A.,
 730 Loustau, D., McGrath, M.J., Meyfroidt, P., Moors, E.J., Naudts, K., Novick, K., Otto, J., Pilegaard, K., Pio, C.A., Rambal,
 731 S., Rebmann, C., Ryder, J., Suyker, A.E., Varlagin, A., Wattenbach, M., Dolman, A.J., 2014. Land management and
 732 land-cover change have impacts of similar magnitude on surface temperature. *Nature Climate Change* 4, 389–393. URL:
 733 <https://www.nature.com/articles/nclimate2196>, doi:10.1038/nclimate2196.
- 734 Masson-Delmotte, V., P.Z.A.P.S.L.C.C.P.S.B.N.C.Y.C.L.G.M.I.G.M.H.K.L.E.L.J.B.R.M.T.K.M.T.W.O.Y.R.Y.a.B.Z.e., 2021.
 735 IPCC, 2021: Climate Change 2021: The Physical Science Basis. Contribution of Working Group I to the Sixth Assessment
 736 Report of the Intergovernmental Panel on Climate Change. Technical Report. URL: <https://www.ipcc.ch/>. publication
 737 Title: Cambridge University Press. In Press.
- 738 McEvoy, D.J., Huntington, J.L., Hobbins, M.T., Wood, A., Morton, C., Anderson, M., Hain, C., 2016. The Evaporative Demand
 739 Drought Index. Part II: CONUS-Wide Assessment against Common Drought Indicators. *Journal of Hydrometeorology* 17,
 740 1763–1779. URL: <http://journals.ametsoc.org/doi/10.1175/JHM-D-15-0122.1>, doi:10.1175/JHM-D-15-0122.1.
- 741 Meroni, M., Rembold, F., Fasbender, D., Vrieling, A., 2017. Evaluation of the Standardized Precipitation Index as an early
 742 predictor of seasonal vegetation production anomalies in the Sahel. *Remote Sensing Letters* 8, 301–310. URL: <http://www.tandfonline.com/doi/abs/10.1080/2150704X.2016.1264020>, doi:10.1080/2150704X.2016.1264020.
- 743 Miranda, A., Altamirano, A., Cayuela, L., Lara, A., González, M., 2017. Native forest loss in the Chilean biodiversity hotspot:
 744 revealing the evidence. *Regional Environmental Change* 17, 285–297. URL: <http://link.springer.com/10.1007/s10113-016-1010-7>, doi:10.1007/s10113-016-1010-7.
- 745 Miranda, A., Lara, A., Altamirano, A., Di Bella, C., González, M.E., Julio Camarero, J., 2020. Forest browning trends in
 746 response to drought in a highly threatened mediterranean landscape of South America. *Ecological Indicators* 115, 106401.
 747 URL: <https://linkinghub.elsevier.com/retrieve/pii/S1470160X20303381>, doi:10.1016/j.ecolind.2020.106401.
- 748 Muñoz, A.A., Klock-Barría, K., Alvarez-Garreton, C., Aguilera-Betti, I., González-Reyes, .., Lastra, J.A., Chávez, R.O.,
 749 Barría, P., Christie, D., Rojas-Badilla, M., LeQuesne, C., 2020. Water Crisis in Petorca Basin, Chile: The Combined
 750 Effects of a Mega-Drought and Water Management. *Water* 12, 648. URL: <https://www.mdpi.com/2073-4441/12/3/648>, doi:10.3390/w12030648.
- 751 Muñoz-Sabater, J., Dutra, E., Agustí-Panareda, A., Albergel, C., Arduini, G., Balsamo, G., Boussetta, S., Choulga, M.,
 752 Harrigan, S., Hersbach, H., Martens, B., Miralles, D.G., Piles, M., Rodríguez-Fernández, N.J., Zsoter, E., Buontempo, C.,
 753 Thépaut, J.N., 2021. ERA5-Land: a state-of-the-art global reanalysis dataset for land applications. *Earth System Science*

- 766 Data 13, 4349–4383. URL: <https://essd.copernicus.org/articles/13/4349/2021/>, doi:10.5194/essd-13-4349-2021.
- 767 Narasimhan, B., Srinivasan, R., 2005. Development and evaluation of Soil Moisture Deficit Index (SMDI) and Evapotranspiration Deficit Index (ETDI) for agricultural drought monitoring. Agricultural and Forest Meteorology 133, 69–88. URL: <https://linkinghub.elsevier.com/retrieve/pii/S0168192305001565>, doi:10.1016/j.agrformet.2005.07.012.
- 770 Nicolai-Shaw, N., Zscheischler, J., Hirschi, M., Gudmundsson, L., Seneviratne, S.I., 2017. A drought event composite analysis using satellite remote-sensing based soil moisture. Remote Sensing of Environment 203, 216–225. URL: <https://linkinghub.elsevier.com/retrieve/pii/S0034425717302729>, doi:10.1016/j.rse.2017.06.014.
- 773 Noguera, I., Vicente-Serrano, S.M., Domínguez-Castro, F., 2022. The Rise of Atmospheric Evaporative Demand Is Increasing Flash Droughts in Spain During the Warm Season. Geophysical Research Letters 49, e2021GL097703. URL: <https://agupubs.onlinelibrary.wiley.com/doi/10.1029/2021GL097703>, doi:10.1029/2021GL097703.
- 776 Paruelo, J.M., Texeira, M., Staiano, L., Mastrángelo, M., Amdan, L., Gallego, F., 2016. An integrative index of Ecosystem Services provision based on remotely sensed data. Ecological Indicators 71, 145–154. URL: <https://www.sciencedirect.com/science/article/pii/S1470160X16303843>, doi:10.1016/j.ecolind.2016.06.054. publisher: Elsevier.
- 779 Pebesma, E., 2018. Simple Features for R: Standardized Support for Spatial Vector Data. The R Journal 10, 439–446. URL: <https://doi.org/10.32614/RJ-2018-009>, doi:10.32614/RJ-2018-009.
- 800 Pebesma, E., Bivand, R., 2023. Spatial Data Science: With applications in R. Chapman and Hall/CRC, London. URL: <https://r-spatial.org/book/>.
- 803 Peng, D., Zhang, B., Wu, C., Huete, A.R., Gonsamo, A., Lei, L., Ponce-Campos, G.E., Liu, X., Wu, Y., 2017. Country-level net primary production distribution and response to drought and land cover change. Science of The Total Environment 574, 65–77. URL: <https://linkinghub.elsevier.com/retrieve/pii/S0048969716319507>, doi:10.1016/j.scitotenv.2016.09.033.
- 806 Pitman, A.J., De Noblet-Ducoudré, N., Avila, F.B., Alexander, L.V., Boisier, J.P., Brovkin, V., Delire, C., Cruz, F., Donat, M.G., Gayler, V., Van Den Hurk, B., Reick, C., Volodko, A., 2012. Effects of land cover change on temperature and rainfall extremes in multi-model ensemble simulations. Earth System Dynamics 3, 213–231. URL: <https://esd.copernicus.org/articles/3/213/2012/>, doi:10.5194/esd-3-213-2012.
- 809 Potopová, V., Stepánek, P., Mozný, M., Türkott, L., Soukup, J., 2015. Performance of the standarised precipitation evapotranspiration index at various lags for agricultural drought risk assessment in the {C}zech {R}epublic. Agricultural and Forest Meteorology 202, 26–38.
- 812 R Core Team, 2023. R: A Language and Environment for Statistical Computing. R Foundation for Statistical Computing, Vienna, Austria. URL: <https://www.R-project.org/>.
- 815 Rhee, J., Im, J., Carbone, G.J., 2010. Monitoring agricultural drought for arid and humid regions using multi-sensor remote sensing data. Remote Sensing of Environment 114, 2875–2887. URL: <http://www.sciencedirect.com/science/article/pii/S003442571000221X>, doi:10.1016/j.rse.2010.07.005.
- 818 Rodríguez-Echeverría, J., Echeverría, C., Oyarzún, C., Morales, L., 2018. Impact of land-use change on biodiversity and ecosystem services in the Chilean temperate forests. Landscape Ecology 33, 439–453. URL: <http://link.springer.com/10.1007/s10980-018-0612-5>, doi:10.1007/s10980-018-0612-5.
- 821 Running, S., Zhao, M., 2019. MOD17A3HGF MODIS/Terra Net Primary Production Gap-Filled Yearly L4 Global 500 m SIN Grid V006. URL: <https://lpdaac.usgs.gov/products/mod17a3hgv006/>, doi:10.5067/MODIS/MOD17A3HGF.006.
- 824 Schulz, J.J., Cayuela, L., Echeverría, C., Salas, J., Rey Benayas, J.M., 2010. Monitoring land cover change of the dryland forest landscape of Central Chile (1975–2008). Applied Geography 30, 436–447. URL: <https://linkinghub.elsevier.com/retrieve/pii/S0143622809000885>, doi:10.1016/j.apgeog.2009.12.003.
- 827 Sen, P.K., 1968. Estimates of the Regression Coefficient Based on Kendall's Tau. Journal of the American Statistical Association 63, 1379–1389. URL: <http://www.tandfonline.com/doi/abs/10.1080/01621459.1968.10480934>, doi:10.1080/01621459.1968.10480934.
- 830 Slette, I.J., Post, A.K., Awad, M., Even, T., Punzalan, A., Williams, S., Smith, M.D., Knapp, A.K., 2019. How ecologists define drought, and why we should do better. Global Change Biology 25, 3193–3200. URL: <https://onlinelibrary.wiley.com/doi/10.1111/gcb.14747>, doi:10.1111/gcb.14747.
- 833 Song, X.P., Hansen, M.C., Stehman, S.V., Potapov, P.V., Tyukavina, A., Vermote, E.F., Townshend, J.R., 2018. Global land change from 1982 to 2016. Nature 560, 639–643. URL: <https://www.nature.com/articles/s41586-018-0411-9>, doi:10.1038/s41586-018-0411-9.
- 836 Souza, A.G.S.S., Ribeiro Neto, A., Souza, L.L.D., 2021. Soil moisture-based index for agricultural drought assessment: SMADI application in Pernambuco State-Brazil. Remote Sensing of Environment 252, 112124. URL: <https://linkinghub.elsevier.com/retrieve/pii/S0034425720304971>, doi:10.1016/j.rse.2020.112124.
- 840 Taucare, M., Viguier, B., Figueiroa, R., Daniele, L., 2024. The alarming state of Central Chile's groundwater resources: A paradigmatic case of a lasting overexploitation. Science of The Total Environment 906, 167723. URL: <https://linkinghub.elsevier.com/retrieve/pii/S0048969723063507>, doi:10.1016/j.scitotenv.2023.167723.
- 843 Tennekes, M., 2018. tmap: Thematic Maps in R. Journal of Statistical Software 84, 1–39. doi:10.18637/jss.v084.i06.
- 846 Urrutia-Jalabert, R., González, M.E., González-Reyes, , Lara, A., Garreaud, R., 2018. Climate variability and forest fires in central and south-central Chile. Ecosphere 9, e02171. URL: <https://esajournals.onlinelibrary.wiley.com/doi/10.1002/ecs2.2171>, doi:10.1002/ecs2.2171.
- 850 Van Loon, A.F., Gleeson, T., Clark, J., Van Dijk, A.I., Stahl, K., Hannaford, J., Di Baldassarre, G., Teuling, A.J., Tallaksen, L.M., Uijlenhoet, R., Hannah, D.M., Sheffield, J., Svoboda, M., Verbeiren, B., Wagener, T., Rangecroft, S., Wanders, N., Van Lanen, H.A., 2016. Drought in the Anthropocene. Nature Geoscience 9, 89–91. doi:10.1038/ngeo2646.
- 853 Van Loon, A.F., Van Huijgevoort, M.H.J., Van Lanen, H.A.J., 2012. Evaluation of drought propagation in an ensemble mean of large-scale hydrological models. Hydrology and Earth System Sciences 16, 4057–4078. URL: <https://hess.copernicus.org/articles/16/4057/2012/>, doi:10.5194/hess-16-4057-2012.

- 831 Venegas-González, A., Juñent, F.R., Gutiérrez, A.G., Filho, M.T., 2018. Recent radial growth decline in response to increased
832 drought conditions in the northernmost Nothofagus populations from South America. Forest Ecology and Management 409,
833 94–104. URL: <https://linkinghub.elsevier.com/retrieve/pii/S0378112717313993>, doi:[10.1016/j.foreco.2017.11.006](https://doi.org/10.1016/j.foreco.2017.11.006).
- 834 Venegas-González, A., Muñoz, A.A., Carpintero-Gibson, S., González-Reyes, A., Schneider, I., Gipolou-Zuñiga, T., Aguilera-
835 Betti, I., Roig, F.A., 2023. Sclerophyllous Forest Tree Growth Under the Influence of a Historic Megadrought in the
836 Mediterranean Ecoregion of Chile. Ecosystems 26, 344–361. URL: <https://link.springer.com/10.1007/s10021-022-00760-x>,
837 doi:[10.1007/s10021-022-00760-x](https://doi.org/10.1007/s10021-022-00760-x).
- 838 Vicente-Serrano, S.M., Azorin-Molina, C., Sanchez-Lorenzo, A., Revuelto, J., López-Moreno, J.I., González-Hidalgo, J.C.,
839 Moran-Tejeda, E., Espejo, F., 2014. Reference evapotranspiration variability and trends in Spain, 1961–2011. Global
840 and Planetary Change 121, 26–40. URL: <https://linkinghub.elsevier.com/retrieve/pii/S0921818114001180>, doi:[10.1016/j.gloplacha.2014.06.005](https://doi.org/10.1016/j.gloplacha.2014.06.005).
- 841 Vicente-Serrano, S.M., Beguería, S., López-Moreno, J.I., 2010. A multiscalar drought index sensitive to global warming: The
842 standardized precipitation evapotranspiration index. Journal of Climate 23, 1696–1718. URL: <http://dx.doi.org/10.1175/2009JCLI2909.1>, doi:[10.1175/2009JCLI2909.1](https://doi.org/10.1175/2009JCLI2909.1).
- 843 Vicente-Serrano, S.M., Peña-Angulo, D., Beguería, S., Domínguez-Castro, F., Tomás-Burguera, M., Noguera, I., Gimeno-
844 Sotelo, L., El Kenawy, A., 2022. Global drought trends and future projections. Philosophical Transactions of the Royal
845 Society A: Mathematical, Physical and Engineering Sciences 380, 20210285. URL: <https://royalsocietypublishing.org/doi/10.1098/rsta.2021.0285>, doi:[10.1098/rsta.2021.0285](https://doi.org/10.1098/rsta.2021.0285).
- 846 Vicente-Serrano, S.M., McVicar, T.R., Miralles, D.G., Yang, Y., Tomas-Burguera, M., 2020. Unraveling the influence of
847 atmospheric evaporative demand on drought and its response to climate change. WIREs Climate Change 11, e632. URL:
848 <https://wires.onlinelibrary.wiley.com/doi/10.1002/wcc.632>, doi:[10.1002/wcc.632](https://doi.org/10.1002/wcc.632).
- 849 Wickham, H., Averick, M., Bryan, J., Chang, W., McGowan, L.D., François, R., Golemund, G., Hayes, A., Henry, L., Hester,
850 J., Kuhn, M., Pedersen, T.L., Miller, E., Bache, S.M., Müller, K., Ooms, J., Robinson, D., Seidel, D.P., Spinu, V., Takahashi,
851 K., Vaughan, D., Wilke, C., Woo, K., Yutani, H., 2019. Welcome to the tidyverse. Journal of Open Source Software 4, 1686.
852 doi:[10.21105/joss.01686](https://doi.org/10.21105/joss.01686).
- 853 Wilhite, D.A., Glantz, M.H., 1985. Understanding: The drought phenomenon: The role of definitions. Water International 10,
854 111–120. URL: <http://dx.doi.org/10.1080/02508068508686328>, doi:[10.1080/02508068508686328](https://doi.org/10.1080/02508068508686328).
- 855 Wilks, D.S., 2011. Empirical distributions and exploratory data analysis. Statistical Methods in the Atmospheric Sciences 100.
- 856 Winkler, K., Fuchs, R., Rounsevell, M., Herold, M., 2021. Global land use changes are four times greater than previously
857 estimated. Nature Communications 12, 2501. URL: <https://www.nature.com/articles/s41467-021-22702-2>, doi:[10.1038/s41467-021-22702-2](https://doi.org/10.1038/s41467-021-22702-2).
- 858 WMO, Svoboda, M., Hayes, M., Wood, D.A., 2012. Standardized Precipitation Index User Guide. WMO, Geneva. URL:
859 http://library.wmo.int/opac/index.php?lvl=notice_display&id=13682. series Title: WMO Publication Title: WMO-No.
860 1090 © Issue: 1090.
- 861 Wright, M.N., Ziegler, A., 2017. ranger: A Fast Implementation of Random Forests for High Dimensional Data in C++ and
862 R. Journal of Statistical Software 77, 1–17. doi:[10.18637/jss.v077.i01](https://doi.org/10.18637/jss.v077.i01).
- 863 Wu, C., Zhong, L., Yeh, P.J.F., Gong, Z., Lv, W., Chen, B., Zhou, J., Li, J., Wang, S., 2024. An evaluation framework
864 for quantifying vegetation loss and recovery in response to meteorological drought based on SPEI and NDVI. Science of
865 The Total Environment 906, 167632. URL: <https://linkinghub.elsevier.com/retrieve/pii/S0048969723062599>, doi:[10.1016/j.scitotenv.2023.167632](https://doi.org/10.1016/j.scitotenv.2023.167632).
- 866 Xiao, C., Zaehle, S., Yang, H., Wigneron, J.P., Schmullius, C., Bastos, A., 2023. Land cover and management effects on
867 ecosystem resistance to drought stress. Earth System Dynamics 14, 1211–1237. URL: <https://esd.copernicus.org/articles/14/1211/2023/>, doi:[10.5194/esd-14-1211-2023](https://doi.org/10.5194/esd-14-1211-2023).
- 868 Yang, J., Huang, X., 2021. The 30 m annual land cover dataset and its dynamics in China from 1990 to 2019. Earth System
869 Science Data 13, 3907–3925. URL: <https://essd.copernicus.org/articles/13/3907/2021/>, doi:[10.5194/essd-13-3907-2021](https://doi.org/10.5194/essd-13-3907-2021).
- 870 Zambrano, F., 2023a. Data of monthly climate variables and drought indices within continental Chile for 1981–2023. URL:
871 <https://zenodo.org/doi/10.5281/zenodo.10359546>, doi:[10.5281/ZENODO.10359546](https://doi.org/10.5281/ZENODO.10359546).
- 872 Zambrano, F., 2023b. Four decades of satellite data for agricultural drought monitoring throughout the growing season in
873 Central Chile, in: Vijay P. Singh Deepak Jhajharia, R.M., Kumar, R. (Eds.), Integrated Drought Management, Two Volume
874 Set. CRC Press, p. 28.
- 875 Zambrano, F., Lillo-Saavedra, M., Verbist, K., Lagos, O., 2016. Sixteen years of agricultural drought assessment of the
876 biobío region in chile using a 250 m resolution vegetation condition index (VCI). Remote Sensing 8, 1–20. URL: <http://www.mdpi.com/2072-4292/8/6/530>, doi:[10.3390/rs8060530](https://doi.org/10.3390/rs8060530). publisher: Multidisciplinary Digital Publishing Institute.
- 877 Zambrano, F., Vrieling, A., Nelson, A., Meroni, M., Tadesse, T., 2018. Prediction of drought-induced reduction of agricultural
878 productivity in Chile from MODIS, rainfall estimates, and climate oscillation indices. Remote Sensing of Environment
879 219, 15–30. URL: <https://www.sciencedirect.com/science/article/pii/S0034425718304541>, doi:[10.1016/j.rse.2018.10.006](https://doi.org/10.1016/j.rse.2018.10.006).
880 publisher: Elsevier.
- 881 Zhao, Y., Feng, D., Yu, L., Wang, X., Chen, Y., Bai, Y., Hernández, H.J., Galleguillos, M., Estades, C., Biging, G.S., Radke,
882 J.D., Gong, P., 2016. Detailed dynamic land cover mapping of Chile: Accuracy improvement by integrating multi-temporal
883 data. Remote Sensing of Environment 183, 170–185. URL: <https://linkinghub.elsevier.com/retrieve/pii/S0034425716302188>,
884 doi:[10.1016/j.rse.2016.05.016](https://doi.org/10.1016/j.rse.2016.05.016).
- 885 Zhou, K., Li, J., Zhang, T., Kang, A., 2021. The use of combined soil moisture data to characterize agricultural drought
886 conditions and the relationship among different drought types in China. Agricultural Water Management 243, 106479. URL:
887 <https://linkinghub.elsevier.com/retrieve/pii/S0378377420305965>, doi:[10.1016/j.agwat.2020.106479](https://doi.org/10.1016/j.agwat.2020.106479).